Int J Earth Sci (Geol Rundsch)
DOI 10.1007/s00531-007-0297-5

ORIGINAL PAPER

Lower Carboniferous post-orogenic granites in central-eastern Sierra de Velasco, Sierras Pampeanas, Argentina: U–Pb monazite geochronology, geochemistry and Sr–Nd isotopes

Pablo Grosse · Frank Söllner · Miguel A. Báez · Alejandro J. Toselli · Juana N. Rossi · Jesus D. de la Rosa

Received: 1 October 2007 / Accepted: 19 December 2007

Abstract The central-eastern part of the Sierra de Velasco (Sierras Pampeanas, NW Argentina) is formed by the large Huaco (40 × 30 km) and Sanagasta (25 × 15 km) granite massifs and the small La Chinchilla stock (2 × 2 km). The larger granites intrude into Ordovician metagranitoids and crosscut Devonian (?) mylonitic shear zones, whereas the small stock sharply intrudes into the Huaco granite. The two voluminous granites are biotitic-muscovitic and biotitic porphyritic syeno- to monzogranites. They contain small and rounded tonalitic and quartz-dioritic mafic microgranular enclaves. The small stock is an equigranular, zinnwaldite- and fluorite-bearing monzogranite. The studied granites are silica-rich (SiO_2 >70%), potassium-rich (K_2O >4%), ferroan, alkali-calcic to slightly calk-alkalic, and moderately to weakly peraluminous (A/CNK: 1.06–1.18 Huaco granite, 1.01–1.09 Sanagasta granite, 1.05–1.06 La Chinchilla stock). They have moderate to strong enrichments in several LIL (Li, Rb, Cs) and HFS (Nb, Ta, Y, Th, U) elements, and low Sr, Ba and Eu contents. U–Pb monazite age determinations indicate Lower Carboniferous crystallization ages: 350–358 Ma for the Huaco granite, 352.7 ± 1.4 Ma for the Sanagasta granite and 344.5 ± 1.4 Ma for the La Chinchilla stock. The larger granites have similar εNd values between −2.1 and −4.3, whereas the younger stock has higher εNd of −0.6 to −1.4, roughly comparable to the values obtained for the Carboniferous San Blas granite (−1.4 to −1.7), located in the north of the sierra. The Huaco and Sanagasta granites have a mainly crustal source, but with some participation of a more primitive, possibly mantle-derived, component. The main crustal component can be attributed to Ordovician peraluminous metagranitoids. The La Chinchilla stock derives from a more primitive source, suggesting an increase with time in the participation of the primitive component during magma genesis. The studied granites were generated during a post-orogenic period in a within-plate setting, possibly as a response to the collapse of the previous Famatinian orogen, extension of the crust and mantle upwelling. They are part of the group of Middle Devonian–Lower Carboniferous granites of the Sierras Pampeanas. The distribution and U–Pb ages of these granites suggests a northward arc-parallel migration of this mainly post-orogenic magmatism with time.

Keywords Carboniferous post-orogenic granites · U–Pb monazite geochronology · Geochemistry · Sr–Nd isotopes · Sierra de Velasco · Sierras Pampeanas · Argentina

P. Grosse (✉)
Instituto Superior de Correlación Geológica (CONICET) and Fundación Miguel Lillo, Miguel Lillo 251, 4000 San Miguel de Tucumán, Argentina
e-mail: pablogrosse@yahoo.com

F. Söllner
Department für Geo- und Umweltwissenschaften, Ludwig-Maximilians-Universität, Luisenstrasse 37, 80333 Munich, Germany

M. A. Báez · A. J. Toselli · J. N. Rossi
Instituto Superior de Correlación Geológica (CONICET) and Facultad de Ciencias Naturales, Universidad Nacional de Tucumán, Miguel Lillo 205, 4000 San Miguel de Tucumán, Argentina

J. D. de la Rosa
Departamento de Geología, Universidad de Huelva, tCampus Universitario El Carmen, 21071 Huelva, Spain

Introduction

The Sierras Pampeanas geological province of northwestern Argentina contains abundant granitoid massifs generated during the Famatinian orogenic cycle (for details see Rapela et al. 2001a; Miller and Söllner 2005). Most of these Famatinian granitoids are related to the main subduction phase of this cycle (e.g. Pankhurst et al. 2000; Rapela et al. 2001a; Miller and Söllner 2005) and have Early-Middle Ordovician ages (e.g. Pankhurst et al. 1998, 2000; Söllner et al. 2001; Höckenreiner et al. 2003) (Fig. 1a). These granitoids are distributed along two subparallel, NNW–SSE trending belts: a main calc-alkaline I-type belt towards the southwest, and an inner peraluminous and S-type belt towards the northeast (Fig. 1a).

Additionally, numerous younger granites of Middle Devonian to Lower Carboniferous age are also present in the Sierras Pampeanas (e.g. Brogioni 1987, 1993; Rapela et al. 1991; Grissom et al. 1998; Llambías et al. 1998; Saavedra et al. 1998; Siegesmund et al. 2004; Dahlquist et al. 2006) (Fig. 1a). The genesis of these granites is not well constrained, and they have been alternatively considered as products of a crustal reheating process during a final phase of the Famatinian cycle, (e.g. Grissom et al. 1998; Llambías et al. 1998; Höckenreiner et al. 2003; Miller and Söllner 2005) or part of a separate cycle called Achalian (e.g. Sims et al. 1998; Rapela et al. 2001a; Siegesmund et al. 2004; López de Luchi et al. 2007).

The Sierra de Velasco is located in the central region of the Sierras Pampeanas (Fig. 1a) and consists almost entirely of rocks of granitoid composition, making it the largest granitic massif of this geological province. The Sierra de Velasco granitoids have generally been regarded as part of the Famatinian inner peraluminous S-type belt (e.g. Rapela et al. 1990; Toselli et al. 1996, 2000; Pankhurst et al. 2000), with the exception of the southern portion of the sierra which seems to correspond to the main calc-alkaline I-type belt (Bellos et al. 2002; Bellos 2005) (Fig. 1a, b). However, field studies carried out in the northern (Báez et al. 2002; Báez and Basei 2005) and central (Grosse and Sardi 2005; Grosse et al. 2005) parts of the sierra indicate the presence of younger undeformed granites (Fig. 1b), possibly belonging to the late-Famatinian, or Achalian, granite group. Recent U–Pb age determinations have confirmed that the northern undeformed granites are of Lower Carboniferous age (Báez et al. 2004; Dahlquist et al. 2006). The central undeformed granites have yet to be dated.

The goal of this study is to determine the absolute ages and the geochemistry of the undeformed granites located in the central part of the Sierra de Velasco. To this end, we have carried out U–Pb dating on monazite and whole-rock elemental and Sr–Nd isotopic geochemical analyses. The obtained data are used to place constraints on the possible magma sources and geotectonic setting of these granites, and to discuss regional implications.

Geological setting: the Sierra de Velasco

The Sierra de Velasco is dominated by rocks of granitoid composition. Low grade metamorphic rocks are only present as small outcrops along the eastern flank of the sierra (Fig. 1b, c). These phyllites and mica schists have been correlated with the La Cébila Formation, located in the Sierra de Ambato (González Bonorino 1951; Espizua and Caminos 1979). Recent discovery of marine fossils in this formation constrains its age to the Lower Ordovician (Verdecchia et al. 2007), in agreement with detrital zircon geochronology (Rapela et al. 2007).

The granitoid units of the Sierra de Velasco have been reviewed and described by Toselli et al. (2000, 2005) and Báez et al. (2005). Two groups can be distinguished (Fig. 1b): older deformed granitoids (here referred to as *metagranitoids*) and younger undeformed granites. The metagranitoids are the most abundant rocks. They are weakly to strongly foliated, depending on the degree of deformation. The main variety consists of strongly peraluminous porphyritic two-mica-, garnet-, sillimanite- and kyanite-bearing meta-monzogranites (Rossi et al. 2000, 2005). Subordinate varieties include strongly peraluminous porphyritic biotite–cordierite meta-monzogranites and moderately peraluminous coarse- to medium-grained biotite meta-granodiorites and meta-tonalites. In the southern part of the sierra, the main lithologies are metaluminous to weakly peraluminous biotite-hornblende meta-granodiorites and meta-tonalites (Bellos 2005) (Fig. 1b). Two U–Pb SHRIMP determinations indicate Lower Ordovician ages for the metagranitoids (481 ± 3 Ma, Pankhurst et al. 2000; 481 ± 2 Ma, Rapela et al. 2001b).

All of the metagranitoids are cut by several NNW–SSE trending mylonitic shear zones (Fig. 1b). No age determinations exist of these shear zones in the Sierra de Velasco. However, similar mylonitic shear zones in other areas of the Sierras Pampeanas have been dated, with ages varying between the Upper Ordovician and the Upper Devonian (Northrup et al. 1998; Rapela et al. 1998; Sims et al. 1998; López et al. 2000; Höckenreiner et al. 2003). The precise Sm–Nd age of 402 ± 2 Ma (Höckenreiner et al. 2003) obtained on syntectonically grown garnet from mylonites of the Sierra de Copacabana (Fig. 1a), which can be traced directly into the Sierra de Velasco (López and Toselli 1993; Söllner et al. 2003), can be considered the best age estimate of mylonitization in this range.

The undeformed granites crop out in the northern and central-eastern parts of the sierra (Fig. 1b). Toselli et al.

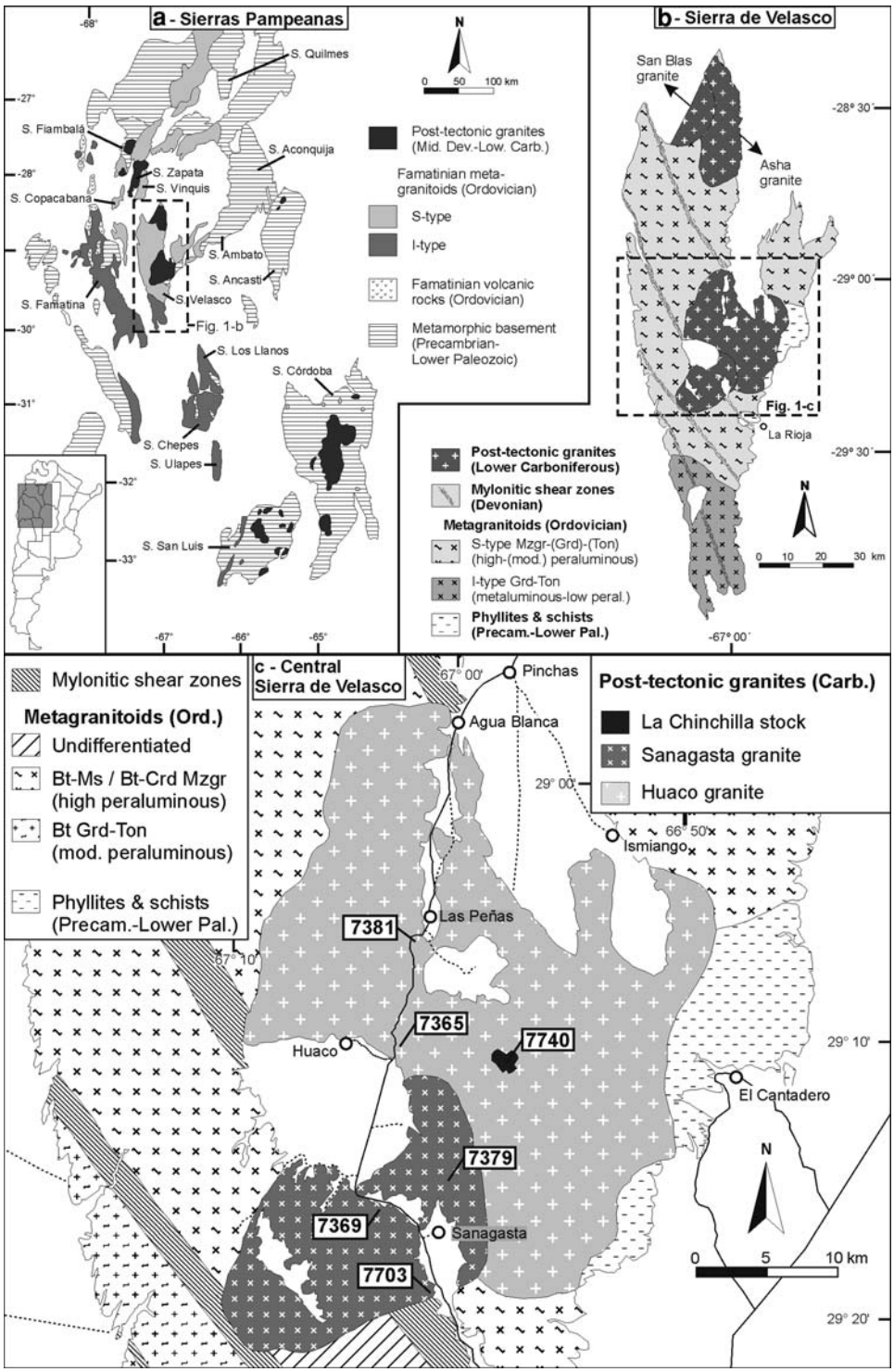

Fig. 1 **a** General geological map of the Sierras Pampeanas of NW Argentina with the main lithologies; sierras considered in the text are named. **b** General geology of the Sierra de Velasco; **c** Geological map of the central part of the Sierra de Velasco showing the Huaco, Sanagasta and La Chinchilla granites, with locations of dated samples; *Bt* biotite, *Ms* muscovite, *Crd* cordierite, *Mzgr* monzogranite, *Ton* tonalite, *Grd* granodiorite

(2006) have grouped these granites in the Aimogasta batholith. The northern San Blas and Asha granites intrude the older metagranitoids and cross-cut the mylonitic shear zones (Báez et al. 2002; Báez and Basei 2005). They are moderately to weakly peraluminous porphyritic two-mica monzogranites. Existing U–Pb ages are 334 ± 5 Ma (conventional U–Pb method on zircon, Báez et al. 2004) and 340 ± 3 Ma (U–Pb SHRIMP on zircon, Dahlquist et al. 2006) for the San Blas granite, and 344 ± 1 Ma (conventional U–Pb method on monazite, Báez et al. 2004) for the Asha granite.

In restricted areas, the granitic rocks are unconformably overlain by continental sandstones and conglomerates of the Paganzo Group (Salfity and Gorustovich 1984), of

Upper Carboniferous to Permian age, deposited during regional uplift of the Sierras Pampeanas. Unconsolidated Tertiary-recent sediments, related to Andean tectonics, locally fill basins and form fluvial terraces and cones.

The Huaco, Sanagasta and La Chinchilla granites

The central-eastern region of the Sierra de Velasco is formed mainly by two large granitic massifs, the Huaco granite (HG) and the Sanagasta granite (SG) (Fig. 1c) (Grosse and Sardi 2005). These granites consist of adjacent, sub-elipsoidal bodies with dimensions of approximately 40 × 30 km for the HG and 25 × 15 km for the SG. Additionally, a small stock of around 2 × 2 km, named La Chinchilla stock (LCS), has been recognized in the central area of the HG (Fig. 1c) (Grosse et al. 2005).

The HG and the SG intrude into the older metagranitoids and mylonites and are not deformed. The contacts are sharp and the granites truncate both the structures of the metagranitoids and the mylonitic shear zones, and contain enclaves of both of these host rocks. These field relationships indicate that the granites are younger than both the crystallization of the metagranitoids and their deformation. The contact between the HG and the SG is irregular and transitional, suggesting that the two granites have similar ages and consist of two coeval magmatic pulses. The transitional area between the two granites is of ~100–200 m; in Fig. 1c the contact between the granites was drawn along this transitional zone. The LCS clearly intrudes into the HG and is thus younger. The contacts are sharp and straight, and aplitic dykes from the LCS commonly cut through the HG.

Both the HG and the SG are rather homogeneous porphyritic syeno- to monzogranites. They are characterized by abundant K-feldspar megacrysts up to 12 cm long (generally between 2 and 5 cm) set in a medium- to coarse-grained groundmass of quartz, plagioclase, K-feldspar, micas and accessory minerals. The megacrysts are usually oriented, defining a primary magmatic foliation.

The HG consists in grayish-white K-feldspar megacrysts (30–36 vol.%) and a groundmass of anhedral quartz (25–39%), subhedral plagioclase laths ($An_{10–23}$) (18–31%), interstitial perthitic K-feldspar (2–14%), dark brown to straw-colored biotite (4–10%) and muscovite (2–6%). Accessory minerals include apatite (up to 0.5%), zircon, monazite and ilmenite, all of which are generally associated with, or included in, biotite.

The SG contains pink K-feldspar megacrysts (33–37%) that are occasionally mantled by plagioclase generating a Rapakivi-like texture. The groundmass consists in anhedral quartz (23–34%), subhedral plagioclase laths ($An_{18–24}$) (17–33%), interstitial perthitic K-feldspar (2–17%), and dark brown to straw-colored biotite (3–10%). Muscovite is absent or very scarce (0–2%). Accessory minerals are commonly found included in biotite. Apatite is less abundant than in the HG, whereas zircon, monazite and especially the opaque minerals (both ilmenite and magnetite) are more frequent. In addition, titanite and allanite are sometimes present.

Both the HG and the SG commonly contain small and rounded mafic microgranular enclaves. These generally have ovoid shapes, elongated parallel to the magmatic flow direction. The enclaves are fine- to very fine-grained equigranular tonalites and quartz-diorites. They contain abundant biotite (15–50%) forming small, subhedral crystals. Opaque minerals and acicular apatite are common. The enclaves usually contain much larger xenocrysts of quartz, feldspar or biotite, and have chilled margins, suggesting partial assimilation and homogenization with the enclosing granites.

Pegmatites and aplites are very common in these granites, specially in the HG. The larger pegmatites are zoned and belong to the rare-element class, beryl type, beryl-columbite-phosphate sub-type with a hybrid LCT-NYF affiliation (Galliski 1993; Sardi 2005; Sardi and Grosse 2005). The HG also contains a small outcrop of an orbicular granite (Quartino and Villar Fabre 1962; Grosse et al. 2006b).

The LCS is a medium-grained, equigranular to slightly porphyritic, monzogranite. It shows a weak textural zonation determined by a progressive increase in grain size towards the center of the stock, where a slight porphyritic texture is present (up to 10% of K-feldspar megacrysts). Mineralogically, the LCS consists of quartz (37–42%), plagioclase (almost pure albite, $An_{1–2}$) (25–33%), K-feldspar (19–34%), discolored, very pale brown to pale red-brown biotite (4–9%), anhedral and irregularly shaped fluorite (up to 1%) and small quantities of zircon, monazite, opaque minerals and very scarce apatite. Beryl is occasionally present as euhedral prismatic crystals.

Microprobe analyses (Grosse et al. 2006a) indicate that the biotites of the HG and the SG have compositions ranging from Fe-biotites to siderophyllites (according to the classification diagram of Tischendorf et al. 1997) and have high Fe/(Fe + Mg) ratios (0.76–0.82), typical of evolved granites. In the discrimination diagram of Nachit et al. (1985), they plot in the calc-alkaline field. Biotites from de LCS have very high Fe/(Fe + Mg) ratios (0.94–0.97) and are Li-rich. They classify mainly as zinnwaldites and also as protolithionites in the classification diagram of Tischendorf et al. (1997).

Zircons of the HG and the SG have similar morphologies. They correspond mainly to the S17–19 and S22–23 types of Pupin (1980), which are characteristic of calc-alkaline series granites. On the other hand, the zircons

of the LCS are different, with morphologies mostly of the P5-type of Pupin (1980), of primitive alkaline affiliation. The San Blas granite, in the north of the sierra (Fig. 1b), has the same zircon typology as the LCS.

No previous U–Pb age determinations exist of the HG and the SG, while the LCS has not been previously dated by any method. K–Ar and Rb–Sr geochronological studies have been carried out on granites of the Sierra de Velasco, which in some cases correspond to the HG or SG (see compilation in Linares and González 1990). The ages in these studies are very variable, spanning from the Ordovician to the Permian, probably due to the inherent problems of the methods used (low closure temperature, Ar loss, etc.).

Analytical methods

U–Pb geochronology

U–Pb geochronology was carried out at the Department of Earth- and Environmental Sciences, Ludwig-Maximilians-Universität, Munich, Germany. Heavy mineral concentrates, mainly zircons and monazites, were obtained using standard crushing, magnetic separation, and heavy-liquid techniques. For each analyzed sample around 50 monazite crystals were handpicked. Chosen crystals were yellow, translucent, anhedral to subhedral and lacked inclusions and fractures. We chose to analyze monazites because this mineral generally does not contain inherited cores and does not suffer radiogenic Pb loss at low temperatures, both common problems in zircons (see Parrish 1990 for discussion). Additionally, the closing temperature of monazite, although slightly lower than that of zircon (for details see Romer and Rötzler 2001), is sufficiently high to maintain the system unperturbed by low-temperature post-crystallization events.

The monazite fractions were cleaned with purified 6 N HCl, H_2O and acetone, and then deposited in Teflon inserts together with a mixed ^{205}Pb–^{233}U spike. Subsequently, samples were dissolved in autoclaves, heated at 180°C, for 5 days using 48% HF and subsequently 6 N HCl. The U and Pb of the samples were separated using small 50 µl ion exchange columns with Dowex raisin AG 1 × 8 100–200 mesh. The isotopic ratios of Pb and U were determined with a thermal ionization mass spectrometer (TIMS) Finnigan MAT 261/262. Pb isotopes were measured in static mode and U isotopes in dynamic mode. Standards (NBS 982Pb and U500) were used for measurement control. U–Pb data was treated using the PBDAT 1.24 (Ludwig 1994) and ISOPLOT/Ex 2.49x (Ludwig 2001) programs. Errors quoted are at the 2σ confidence level. The corrections for initial non-radiogenic Pb was obtained following the model of Stacey and Kramers (1975). The U decay constants proposed by the IUGS (Steiger and Jäger 1977) were used for the age calculations. Mass fractionation was corrected using $0.13 \pm 0.06\%$/a.m.u. for Pb and $0.05 \pm 0.04\%$ per a.m.u for U. Together with the samples, a procedural blank was analyzed to determine the level of contamination. For Pb blank corrections a mean value of 0.2 ng and an isotopic composition of $^{208}Pb/^{204}Pb = 38.14$; $^{207}Pb/^{204}Pb = 15.63$; $^{206}Pb/^{204}Pb = 18.15$ was used. Long term measured standards gave values of: NBS 982 (Pb): $^{208}Pb/^{206}Pb = 0.99474 \pm 0.00013$ (0.013%, $2\sigma_m$, $n = 94$); U500 (U): $^{238}U/^{235}U = 1.00312 \pm 0.00027$ (= 0.027%, $2\sigma_m$, $n = 14$).

Whole-rock major and trace element geochemistry

Whole-rock geochemistry was determined at the universities of Oviedo (major elements) and Huelva (trace elements), Spain. Major elements were analyzed by X-ray fluorescence (XRF) with a Phillips PW2404 system using glass beads. The typical precision of this method is better than ±1.5% relative. Trace elements were analyzed by inductively coupled plasma mass spectrometry (ICP-MS) with an HP-4500 system. Samples were dissolved using a mixture of HF + HNO_3 (8:3), a second dissolution in HNO_3 after evaporation and final dissolution in HCl. The precision and accuracy for most elements is between 5 and 10% relative (5–7% for Rb, Sr, Nd and Sm) and was controlled by repeated analyses of international rock standards SARM-1 (granite) and SARM-4 (norite). Details on the method can be found in de la Rosa et al. (2001).

Sr and Nd isotope geochemistry

Sr and Nd isotope analyses were carried out at the Department of Earth- and Environmental Sciences, Ludwig-Maximilians-Universität, Munich, Germany. The analyzed powders were the same as those used for major and trace element analyses. For the determination of concentrations and for comparison with the ICP-MS data, a mixed Sm–Nd spike was added to 12 samples. For the remaining samples, and for all Rb–Sr calculations, the concentrations obtained by ICP-MS were used.

Samples (approximately 0.1 g each) were dissolved on a hot plate (140°C) during 36 h using a mixture of 5 ml of HF 48% + HNO_3 (5:1). Sr and REE were separated using ion exchange columns with Dowex AG 50W raisin. Nd and Sm were then separated from the total REE fractions using smaller ion exchange columns with bis(2-ethylhexyl)phosphoric acid (HDEHP) and Teflon powder. The

Table 1 U–Pb monazite data of the three studied granites of central-eastern Sierra de Velasco

Sample	Weight (g)	U (ppm)	Th (ppm)	Pb (ppm)	$^{206}Pb/^{204}Pb$ measured	Calculated atomic ratios							Calculated ages (in Ma)					
						$^{206}Pb/^{238}U$	2σ (%)	$^{207}Pb/^{235}U$	2σ (%)	$^{207}Pb/^{206}Pb$	2σ (%)		$^{206}Pb/^{238}U$	2σ	$^{207}Pb/^{235}U$	2σ	$^{207}Pb/^{206}Pb$	2σ
Huaco granite																		
7365Mo	0.000152	10169	83552	1590	7134	0.06809	0.21	0.50217	0.25	0.05349	0.12		424.6	0.9	413.2	1.0	349.7	5.3
7381Mo	0.000138	6135	46863	1469	4343	0.11374	0.21	0.84177	0.24	0.05368	0.11		694.4	1.5	620.1	1.5	357.5	4.9
Sanagasta granite																		
7369Mo	0.000110	30483	830554	1402	3080	0.00592	0.21	0.04348	0.28	0.05330	0.17		38.0	0.1	43.2	0.1	341.5	7.8
7379Mo	0.000093	3311	66434	1049	4023	0.05627	0.21	0.41482	0.26	0.05347	0.15		352.9	0.7	352.3	0.9	348.7	6.7
7703Mo	0.000150	2226	61909	978	3115	0.05631	0.21	0.41196	0.33	0.05306	0.24		353.2	0.7	350.3	1.2	331.3	11.0
La Chinchilla stock																		
7740Mo	0.000122	2681	60110	927	1972	0.05491	0.21	0.40297	0.33	0.05323	0.24		344.6	0.7	343.8	1.1	338.6	10.9

Radiogenic Pb corrected for blank and for initial Pb (following the model of Stacey and Kramers 1975). U corrected for blank. Ages calculated using the PBDAT 1.24 program (Ludwig 1994) and the decay constants recommended by the IUGS (Steiger and Jäger 1977)

isotopic ratios of Sr, Nd and Sm were determined with a thermal ionization mass spectrometer (TIMS) Finnigan MAT 261/262. Standards were used for measurement control (NBS987, AMES Nd and AMES Sm). All errors used are at the 95% (2σ) confidence level. Mass fractionation was corrected normalizing the isotopic ratios to $^{88}Sr/^{86}Sr = 8.3752094$ for Sr, $^{146}Nd/^{144}Nd = 0.7219$ for Nd, and $^{148}Sm/^{152}Sm = 0.4204548$ for Sm. CHUR constants used for εNd calculation were $^{143}Nd/^{144}Nd = 0.512638$ (Goldstein et al. 1984) and $^{147}Sm/^{144}Nd = 0.1967$ (Peucat et al. 1988). One-step model ages were calculated following Goldstein et al. (1984) (with $^{143}Nd/^{144}Nd$ (DM) = 0.51315 and $^{147}Sm/^{144}Nd$ (DM) = 0.217) and two-step model ages were calculated following Liew and Hofmann (1988) (with $^{143}Nd/^{144}Nd$ (DM) = 0.513151, $^{147}Sm/^{144}Nd$ (DM) = 0.219 and $^{147}Sm/^{144}Nd$ (CC) = 0.12). During the period of analyses, the measured standards gave the following average values: NBS987 (Sr): $^{87}Sr/^{86}Sr = 0.710230 \pm 0.000013$ (0.0018%, $2\sigma_m$, $n = 8$); AMES (Nd): $^{143}Nd/^{144}Nd = 0.512131 \pm 0.000007$ (0.0013%, $2\sigma_m$, $n = 10$); AMES (Sm): $^{149}Sm/^{147}Sm = 0.91262 \pm 0.00016$ (0.018%, $2\sigma_m$, $n = 3$).

U–Pb monazite geochronology

Monazite fractions of six samples were analyzed, three of which correspond to the Sanagasta granite (SG), two to the Huaco granite (HG), and one to the La Chinchilla stock (LCS). Locations of the analyzed samples are shown in Fig. 1c. Table 1 shows the analytical results.

In the U–Pb concordia diagram (Fig. 2), two of the six analyzed samples are concordant whereas the other four are discordant, three of which plot above the concordia (phenomenon called "reverse discordance") and one below. Reverse discordance in monazite has been observed by many authors and seems to be a common phenomenon in this mineral (Parrish et al. 1990, and references therein). Schärer (1984) suggests that reverse discordances are owed to an excess in ^{206}Pb due to the decay of ^{230}Th, an intermediate product in the decay chain of ^{238}U to ^{206}Pb, incorporated in significant amounts in the crystal during crystallization of monazite, because this mineral is a carrier of Th. This might be valid for sample 7703Mo, which is slightly reverse discordant (Fig. 2). However, samples 7365Mo, 7381Mo and 7369Mo are strongly reverse and normally discordant, respectively (Fig. 2). These samples probably suffered loss of U (7365Mo, 7381Mo) and radiogenic Pb (7369Mo).

The two samples of the HG are strongly reverse discordant, probably due to loss of U (U contents: 6,135 and 10,129 ppm) (Fig. 2). $^{207}Pb/^{206}Pb$ ages of both samples are equivalent within limits of errors at 350 ± 5 and

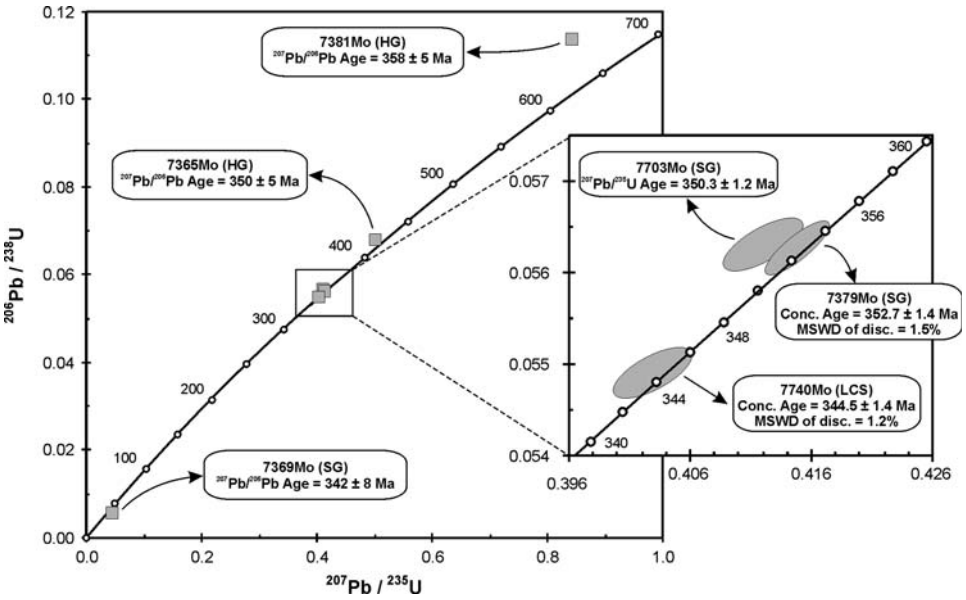

Fig. 2 U–Pb Concordia diagram of monazites from the three studied granites of central-eastern Sierra de Velasco. Two samples correspond to the Huaco granite (HG: 7365Mo and 7381Mo), three to the Sanagasta granite (SG: 7369Mo, 7379Mo and 7703Mo) and one to the La Chinchilla stock (LCS: 7740Mo). See text for further explanations. Plotted error ellipses and quoted errors are at the 2σ confidence level

358 ± 5 Ma. These ages are interpreted as the best estimate for crystallization of the HG. Recently, Söllner et al. (2007) have carried out LA-ICP-MS U–Pb age determinations on zircons of sample 7365 of the HG, obtaining a main crystallization age of 354 ± 4 Ma, thus confirming the monazite $^{207}Pb/^{206}Pb$ ages. In addition, many of these zircons have non-detrital inherited cores with Ordovician ages, suggesting significant participation of Ordovician metagranitoids in the formation of the HG (Söllner et al. 2007).

Only one of the three samples of the SG (sample 7379Mo) gives a concordant age of 352.7 ± 1.4 Ma (degree of discordance = 1.5%, Fig. 2). Sample 7703Mo is slightly reverse discordant at 350.3 ± 1.2 Ma ($^{207}Pb/^{235}U$ age), whereas sample 7369Mo is strongly discordant at 38.0 ± 0.1 Ma ($^{206}Pb/^{238}U$ age; $^{207}Pb/^{206}Pb$ age = 342 ± 8 Ma) (Fig. 2), suggesting loss of radiogenic Pb, possibly related to the very high measured U content (30,483 ppm) and the presence of dim and/or fractured crystals. All three data points, including the origin, fit a regression line with an upper intercept of 340 ± 26 Ma (MSWD = 3.8). The concordant age of 352.7 ± 1.4 Ma of sample 7379Mo is interpreted as the most precise and adequate age of crystallization of the SG.

Sample 7740Mo of the LCS is concordant at 344.5 ± 1.4 Ma (degree of discordance = 1.2%, Fig. 2), which is interpreted as dating the time of crystallization of the LCS.

Geochemistry

Major and trace elements

Table 2 shows 31 whole-rock major and trace element chemical analyses of the studied granites; 13 analyses correspond to the HG, 10 to the SG, 4 to the LCS and 4 to mafic microgranular enclaves of the HG and the SG (see also Grosse et al. 2007). For comparison, the average composition of the border and central facies of the San Blas granite are also shown (calculated from 13 analyses of Báez 2006).

The HG and the SG are characterized by a high and restricted SiO_2 range of 69.7–74.7% (wt%). With slightly lower average SiO_2, the SG has somewhat higher $Fe_2O_3^{tot}$, MgO, TiO_2 and CaO concentrations than the HG, although both granites are poor in these oxides. They are, on the other hand, rich in alkalis (generally >8%), specially in K_2O (generally >5%). Both granites are peraluminous; the HG is mainly moderately peraluminous (Alumina Saturation Index, A/CNK, = 1.06–1.18), whereas the SG is weakly peraluminous (A/CNK = 1.01–1.09).

In major element variation diagrams (Fig. 3), both granites show similar, poorly defined correlations. $Fe_2O_3^{tot}$, MgO and TiO_2 decrease with increasing SiO_2 suggesting fractionation of mafic phases, mainly biotite. Al_2O_3, CaO and P_2O_5 also decrease, suggesting fractionation of plagioclase and apatite, respectively, whereas Na_2O and K_2O do not correlate well with SiO_2.

The HG and the SG can be distinguished well in an A/CNK versus SiO_2 diagram (Fig. 4a) and in the A–B diagram of Debon and Le Fort (1983) (Fig. 4b), due to the different variations in peraluminosity: it decreases with differentiation in the HG, while it increases with differentiation in the SG. These opposite tendencies can be explained by fractionation of muscovite in the HG (which will strongly decrease the peraluminosity of the remaining melt due to its high peraluminosity) and the absence of this mineral in the SG (where the increase in peraluminosity is due mainly to the fractionation of plagioclase, whose A/CNK = 1).

Table 2 Chemical analyses of the studied granites and mafic enclaves of central-eastern Sierra de Velasco, and average composition of the San Blas granite of northern Sierra de Velasco

Unit	Huaco granite												
Sample	6767	6872	6880	6911	6923	7365	7381	7386	7391	7698	7756	6931	7697
Mayor oxides (wt%)													
SiO_2	72.18	73.00	72.47	74.36	73.47	74.40	71.66	74.55	72.59	70.58	74.66	71.99	71.64
TiO_2	0.32	0.32	0.31	0.24	0.18	0.23	0.24	0.18	0.25	0.33	0.21	0.29	0.35
Al_2O_3	14.05	13.80	13.35	12.88	13.80	13.03	14.50	13.18	13.81	14.71	12.94	14.15	14.19
$Fe_2O_3^{tot}$	2.58	2.30	2.70	2.15	1.81	2.39	2.14	1.87	2.26	2.72	2.02	1.92	2.53
MgO	0.38	0.41	0.40	0.33	0.19	0.31	0.32	0.23	0.30	0.50	0.19	0.44	0.38
MnO	0.06	0.06	0.05	0.05	0.05	0.05	0.04	0.04	0.06	0.08	0.05	0.04	0.06
CaO	0.89	0.90	1.05	0.67	0.83	0.78	0.72	0.72	0.73	0.96	0.89	0.88	0.86
Na_2O	3.17	2.89	2.90	2.93	3.08	2.90	3.23	3.07	3.19	3.18	2.86	3.05	3.04
K_2O	5.42	4.87	5.07	4.83	5.83	4.79	5.66	5.19	4.95	5.14	5.42	5.51	5.59
P_2O_5	0.25	0.37	0.28	0.29	0.11	0.19	0.27	0.18	0.25	0.33	0.11	0.25	0.30
P.F.	0.61	1.07	0.87	0.63	0.71	0.55	0.56	0.49	0.66	0.94	0.52	0.75	0.65
Total	99.91	99.99	99.45	99.37	100.05	99.62	99.33	99.70	99.05	99.48	99.87	99.28	99.60
A/(CNK)	1.11	1.18	1.10	1.14	1.07	1.15	1.14	1.10	1.16	1.17	1.06	1.12	1.13
Trace elements (ppm)													
Li	134	246	182	231	160	111	204	194	168	179	84	160	138
Be	16	8.5	15	20	9.4	21	11	13	13	21	6.9	7.2	6.3
Sc	6.8	5.7	5.3	4.3	4.8	5.1	4.1	4.3	4.4	6.8	6.1	3.8	6.8
V	17	25	21	21	4.8	13	13	12	14	18	6.1	25	20
Cr	61	257	36	117	44	51	34	35	61	31	37	24	153
Co	27	34	41	33	30	42	37	32	24	25	30	29	25
Ni	35	10	9.1	10	9.4	17	7.1	8.8	12	34	66	6.9	12
Zn	144	50	69	54	56	66	51	46	70	84	61	47	58
Ga	35	36	36	33	31	27	37	35	28	30	27	42	32
Rb	323	330	329	350	–	269	329	342	294	280	275	290	282
Sr	63	62	58	44	54	46	54	51	42	55	55	81	74
Y	29	24	26	24	29	23	19	25	22	25	36	18	30
Zr	152	76	105	90	118	113	94	90	114	121	102	111	89
Nb	43	33	38	37	36	35	33	38	36	34	31	23	27
Cs	31	44	38	63	27	18	34	41	28	37	11	26	31
Ba	229	225	223	158	222	151	187	176	155	186	205	368	268
La	42	28	39	30	34	31	26	27	31	32	46	43	34
Ce	87	60	82	65	74	65	57	58	66	72	94	89	73
Pr	12	7.2	11	7.9	9.9	8.9	7.1	6.9	9.0	9.4	13	12	9.8
Nd	47	33	48	36	35	34	31	31	35	37	48	52	39
Sm	9.7	7.2	10	7.8	7.8	7.2	7.0	7.2	7.2	7.8	9.6	11	7.7
Eu	1.0	0.71	0.81	0.49	1.0	0.67	0.62	0.55	0.74	0.83	0.91	0.75	1.1
Gd	8.1	6.4	8.4	6.8	6.8	6.6	6.1	6.4	6.0	7.1	8.0	7.7	7.0
Tb	1.3	0.87	1.1	0.95	1.2	1.1	0.78	0.94	1.0	1.1	1.4	0.85	1.2
Dy	6.4	5.5	6.5	5.6	6.2	5.6	4.8	5.7	5.2	6.0	7.6	4.5	6.5
Ho	1.1	0.86	0.93	0.84	1.2	0.90	0.68	0.84	0.84	1.0	1.4	0.63	1.2
Er	2.5	2.4	2.4	2.2	3.2	2.1	1.8	2.2	2.0	2.5	4.1	1.7	3.3
Tm	0.34	0.21	0.17	0.17	0.48	0.27	0.13	0.16	0.29	0.37	0.63	0.11	0.48
Yb	2.0	2.0	1.7	1.7	2.9	1.6	1.5	1.6	1.6	2.2	3.8	1.3	2.9
Lu	0.30	0.14	0.12	0.12	0.44	0.23	0.082	0.11	0.23	0.34	0.58	0.078	0.45
Ta	7.8	12	12	13	6.1	6.7	13	12	4.8	6.0	4.4	9.1	5.5

Table 2 continued

Unit	Huaco granite												
Sample	6767	6872	6880	6911	6923	7365	7381	7386	7391	7698	7756	6931	7697
Pb	39	27	30	25	35	29	32	30	28	29	35	32	29
Th	31	20	32	25	30	28	23	25	27	27	43	33	29
U	7.6	6.9	9.7	7.9	5.2	9.2	8.2	9.6	7.1	7.4	7.5	4.5	6.1
K/Rb	139	123	128	115	–	148	143	126	140	153	164	158	165
Rb/Sr	5.1	5.3	5.7	8.0	–	5.9	6.1	6.8	7.1	5.0	5.0	3.6	3.8
Σ REE	220	154	212	165	185	164	145	148	166	180	239	224	187
Eu/Eu*	0.35	0.32	0.27	0.21	0.43	0.30	0.29	0.25	0.34	0.34	0.32	0.26	0.47
$(La/Yb)_N$	14	9.4	15	11	7.8	13	12	11	13	10	8.1	22	7.8
Unit	Sanagasta granite												
Sample	6659	6889	6890	7115	7251	7354	7369	7379	7703	7724			
Mayor oxides (wt%)													
SiO_2	72.96	73.91	74.54	71.06	73.37	72.33	69.65	72.03	70.87	74.10			
TiO_2	0.26	0.23	0.23	0.50	0.30	0.21	0.56	0.32	0.47	0.30			
Al_2O_3	13.52	13.63	12.33	13.56	13.38	14.21	13.49	13.92	13.79	13.23			
$Fe_2O_3^{tot}$	2.09	2.01	2.24	2.96	2.49	2.03	3.95	2.48	2.86	1.87			
MgO	0.26	0.26	0.28	0.70	0.27	0.18	0.64	0.33	0.55	0.39			
MnO	0.06	0.04	0.04	0.06	0.05	0.05	0.06	0.05	0.07	0.04			
CaO	0.90	1.08	0.77	1.45	0.87	0.90	1.48	1.21	1.42	1.04			
Na_2O	3.00	2.99	2.81	2.86	2.80	3.30	2.97	3.01	2.90	2.80			
K_2O	5.65	5.60	4.90	5.43	5.81	5.94	5.35	5.77	5.14	5.36			
P_2O_5	0.15	0.11	0.14	0.21	0.15	0.13	0.31	0.19	0.21	0.14			
P.F.	0.54	0.39	0.45	0.65	0.62	0.49	0.65	0.58	0.85	0.65			
Total	99.38	100.24	98.72	99.44	100.11	99.77	99.11	99.88	99.12	99.92			
A/(CNK)	1.07	1.05	1.09	1.03	1.07	1.05	1.01	1.04	1.07	1.07			
Trace elements (ppm)													
Li	76	74	90	56	80	129	97	102	64	64			
Be	8.8	6.0	8.4	3.6	7.4	11	6.1	11	4.8	4.0			
Sc	9.0	4.6	4.7	8.1	6.6	4.7	10.2	6.0	9.1	6.6			
V	12	8.8	11	35	15	6.6	41	18	31	18			
Cr	50	28	38	76	71	23	195	34	21	36			
Co	28	22	21	25	25	24	28	37	25	24			
Ni	17	7.8	11	22	30	6.3	9.1	8.9	15	77			
Zn	44	46	135	70	80	48	71	41	51	48			
Ga	33	30	21	37	32	42	43	41	31	27			
Rb	263	257	260	194	275	318	276	296	213	215			
Sr	67	73	44	110	72	79	97	88	89	77			
Y	21	27	23	32	40	27	47	31	27	22			
Zr	140	107	107	110	153	99	170	100	98	86			
Nb	25	24	26	21	32	36	41	30	26	18			
Cs	21	7.7	19	7.6	21	29	12	22	11	8.7			
Ba	299	289	129	408	286	331	366	360	310	257			
La	38	48	29	61	64	47	61	49	48	36			
Ce	78	98	64	119	123	96	121	98	95	76			
Pr	11	13	8.4	17	18	13	17	13	13	10			
Nd	40	47	32	65	68	56	77	57	50	38			
Sm	7.9	9.3	7.0	12	13	12	17	12	9.4	7.1			

Table 2 continued

Unit	Sanagasta granite									
Sample	6659	6889	6890	7115	7251	7354	7369	7379	7703	7724
Eu	1.1	1.3	0.70	1.4	1.3	1.2	1.3	1.3	1.2	0.95
Gd	6.4	7.6	6.1	9.5	10	9.2	15	10	7.6	5.7
Tb	1.0	1.2	1.0	1.5	1.7	1.2	2.1	1.4	1.2	0.90
Dy	5.2	6.2	5.4	7.6	9.3	6.9	12	7.8	6.2	4.8
Ho	0.90	1.2	0.99	1.4	1.7	1.1	2.0	1.2	1.1	0.88
Er	2.2	2.9	2.5	3.5	4.6	2.9	5.2	3.3	3.0	2.4
Tm	0.32	0.42	0.37	0.48	0.69	0.27	0.57	0.34	0.44	0.36
Yb	1.9	2.4	2.3	2.6	4.0	2.4	3.9	2.6	2.5	2.2
Lu	0.28	0.34	0.33	0.41	0.61	0.21	0.42	0.26	0.38	0.35
Ta	4.9	3.1	4.2	2.8	5.8	8.7	8.2	10	3.7	2.8
Pb	32	36	33	38	39	38	38	38	33	34
Th	30	39	33	46	54	37	51	39	40	32
U	5.2	3.6	8.0	4.1	11	7.4	6.9	8.7	4.8	5.0
K/Rb	178	180	157	233	176	155	161	162	200	207
Rb/Sr	4.0	3.5	5.9	1.8	3.8	4.0	2.9	3.4	2.4	2.8
Σ REE	194	239	159	302	319	249	336	258	239	186
Eu/Eu*	0.48	0.49	0.33	0.41	0.34	0.37	0.26	0.36	0.43	0.46
$(La/Yb)_N$	14	14	8.5	15	11	13	10	12	13	11

Unit	La Chinchilla stock				Mafic enclaves				Avg. San Blas granite[a]	
Sample	6916	7738	7739	7740	6877	7728	7734	6885	Border facies	Central facies
Mayor oxides (wt%)										
SiO_2	75.89	76.21	75.40	75.38	70.49	54.94	62.98	54.53	68.99	75.02
TiO_2	0.06	0.07	0.11	0.07	0.54	2.51	1.19	2.66	0.59	0.14
Al_2O_3	12.86	13.16	13.30	13.29	14.29	14.52	15.65	14.84	14.61	13.14
$Fe_2O_3^{tot}$	1.17	1.13	1.28	1.33	4.13	13.82	8.41	13.30	3.71	1.56
MgO	0.09	0.06	0.11	0.06	0.61	2.37	1.22	2.82	0.95	0.10
MnO	0.06	0.04	0.06	0.07	0.10	0.24	0.14	0.29	0.07	0.06
CaO	0.55	0.51	0.40	0.61	1.17	1.82	2.20	2.69	1.71	0.62
Na_2O	3.82	4.21	3.67	3.80	3.33	2.50	4.41	2.73	2.98	3.42
K_2O	4.58	4.20	4.61	4.80	4.87	4.50	2.83	4.38	4.84	4.95
P_2O_5	0.02	0.04	0.07	0.04	0.42	0.85	0.60	0.88	0.35	0.09
P.F.	0.69	0.47	0.70	0.51	0.51	1.03	0.74	0.78	1.17	0.95
Total	99.80	100.09	99.70	99.95	100.46	99.09	100.37	99.91	100.28	100.20
A/(CNK)	1.05	1.06	1.13	1.06	1.11	1.18	1.09	1.05	1.11	1.09
Trace elements (ppm)										
Li	248	136	197	298	279	–	311	556	–	–
Be	12	17	15	80	7.6	13	12	20	12	11
Sc	3.3	3.6	4.5	3.6	8.1	26	17	23	9.8	4.1
V	29	3.8	6.8	6.5	40	171	45	184	55	11
Cr	48	30	18	42	9.0	21	8.5	28	34	29
Co	41	27	25	27	21	25	20	33	47	55
Ni	10	39	49	34	6.8	38	14	28	–	–
Zn	36	47	50	59	132	414	195	234	68	32
Ga	37	27	28	28	28	36	33	48	21	25
Rb	707	360	390	439	–	–	356	758	324	524
Sr	10	16	24	11	44	26	49	85	92	31

Table 2 continued

Unit	La Chinchilla stock				Mafic enclaves				Avg. San Blas granite[a]	
Sample	6916	7738	7739	7740	6877	7728	7734	6885	Border facies	Central facies
Y	88	53	31	78	34	49	51	58	41	72
Zr	83	96	92	99	135	251	339	200	235	156
Nb	66	53	45	61	54	65	59	43	25	48
Cs	27	25	27	32	37	175	47	71	28	27
Ba	39	39	85	36	137	118	123	348	331	105
La	17	20	25	21	39	49	63	45	46	43
Ce	43	49	55	55	84	98	122	97	100	96
Pr	5.8	7.1	7.5	7.9	12	15	19	14	11	11
Nd	29	29	29	34	46	65	77	71	45	41
Sm	11	8.4	7.4	10	10	14	15	15	9.3	9.6
Eu	0.030	0.23	0.35	0.19	0.78	1.2	1.3	1.7	1.2	0.46
Gd	11	7.7	5.8	9.7	9.3	13	14	15	7.5	8.8
Tb	2.2	1.5	1.0	1.9	1.5	2.1	2.3	2.2	1.3	1.9
Dy	15	9.2	5.5	12	8.0	12	12	13	7.2	12
Ho	3.1	1.9	1.0	2.4	1.5	2.2	2.2	2.6	1.4	2.4
Er	9.8	5.8	2.9	7.3	3.5	5.4	5.7	7.2	3.9	7.6
Tm	1.5	1.0	0.48	1.3	0.48	0.74	0.80	0.88	0.59	1.3
Yb	11	7.4	3.3	8.2	2.6	4.2	4.9	6.2	3.6	8.3
Lu	1.6	1.2	0.53	1.3	0.38	0.62	0.73	0.78	0.49	1.2
Ta	26	13	6.2	14	6.8	7.3	5.4	6.4	6.6	14
Pb	52	40	39	53	28	25	19	10	21	31
Th	45	38	38	45	32	24	28	16	29	52
U	69	18	24	49	15	11	11	12	3.8	27
K/Rb	54	97	98	91	–	–	66	48	124	78
Rb/Sr	72	23	16	40	–	–	7.3	8.9	3.5	17
Σ REE	161	150	145	172	219	282	340	293	238	243
Eu/Eu*	0.008	0.086	0.16	0.058	0.25	0.26	0.28	0.34	0.47	0.20
$(La/Yb)_N$	1.0	1.8	5.0	1.7	9.9	7.7	8.6	4.9	9.2	5.0

[a] Data from 13 analyses of Báez (2006)

The LCS is weakly peraluminous (A/CNK = 1.05–1.06; except one sample with a value of 1.13) with elevated SiO_2 contents (75.4–76.2%). It has very low contents of CaO, P_2O_5 and ferromagnesian oxides, specially MgO (Fig. 3). The alkali contents are similar to that of the HG and SG, although the LCS has higher Na_2O and lower K_2O concentrations (Fig. 3).

All three granites are ferroan (Fig. 5a), alkali-calcic to slightly calk-alkalic (Fig. 5b) and potassium-rich (Fig. 3). In the A–B diagram of Debon and Le Fort (1983), with the fields of Villaseca et al. (1998a) (Fig. 4b), the HG is classified as moderately peraluminous, the SG as low peraluminous and the LCS as a felsic peraluminous granite.

The HG and the SG have similar overall trace element concentrations; high contents of several LIL (Li, Rb, Cs) and HFS (Nb, Ta, Th, U) elements and of Zn and Ga, and low contents of Sr and Ba. The HG has higher concentrations in Li, Rb, Cs and U, whereas the SG is richer in Sr, Ba, Y, Th and the REE. These differences suggest that the HG is more evolved than the SG, in accordance with their major element contents. The more evolved character of the HG is also indicated by its lower K/Rb ratios (HG = 115–165; SG = 155–233) and higher Rb/Sr ratios (HG = 3.6–8.0; SG = 1.8–5.9).

The LCS is characterized by elevated concentrations of many trace elements and very low concentrations of some others. Compared to the HG and the SG, the LCS is enriched in Li, Rb, Nb, Ta, U, Y and the HREE, and it is impoverished in Sr, Ba and Eu. The enrichment in U is especially noticeable, with values (18–69 ppm) much higher than that of normal granites (4 ppm, Rogers and Adams 1969). The LCS also has very low K/Rb ratios (54–98) and very high Rb/Sr ratios (16–72). Although F was not analyzed, the presence of fluorite suggests high F contents.

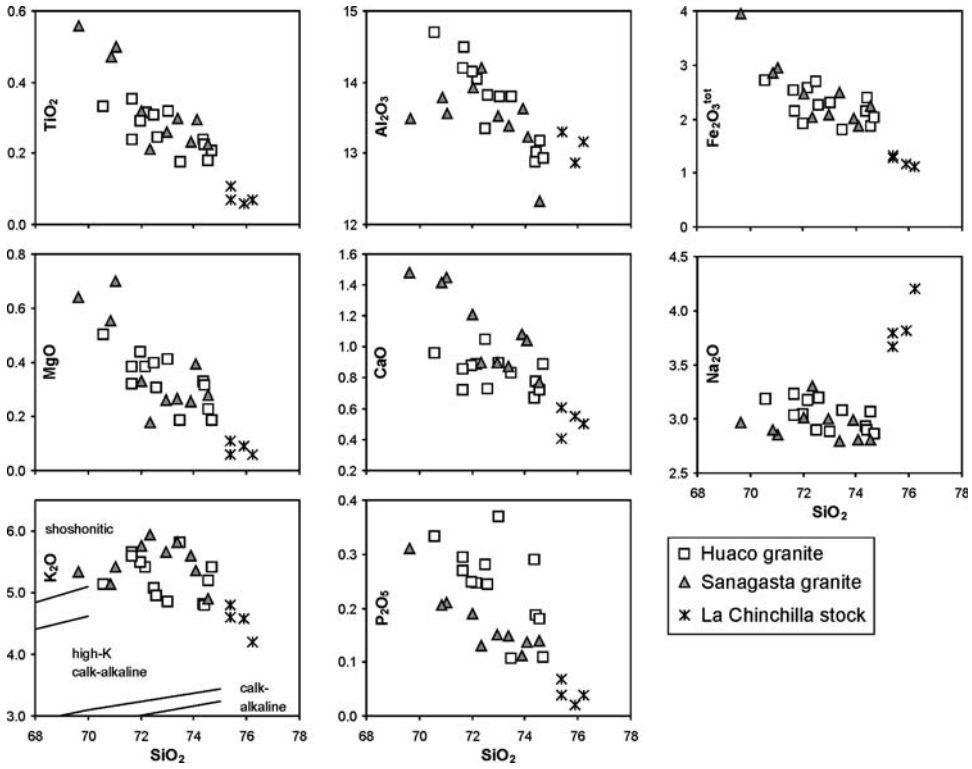

Fig. 3 Variation diagrams of major oxides versus SiO_2. In the K_2O diagram the divisions are from Rickwood (1989)

The major and trace element contents of the LCS indicate that it is a highly evolved leucogranite.

The HG and the SG define similar patterns in a multi-element spider diagram normalized to the primitive mantle (McDonough et al. 1992) (Fig. 6). They both show Rb, Th and Ta positive anomalies, Ba and Sr negative anomalies, and smoothly decreasing values between La and Lu (Fig. 6). Compared to the composition of the crust of Taylor and McLennan (1985), the HG and the SG have higher concentrations in most elements (Rb, Th, U, K, Nb, Ta and the LREE), similar Ba, Zr, Y and HREE contents, and a lower Sr value (Fig. 6). The LCS shows, in general terms, a similar pattern as the HG and the SG, but is distinguished by the stronger U positive anomaly and Ba and Sr negative anomalies, and by the higher concentrations in Nb, Ta and specially Y and the HREE (Fig. 6).

The HG and the SG show similar chondrite-normalized REE patterns, although the SG has higher overall concentrations (Fig. 7). The REE of both granites are moderately fractionated, with $(La/Yb)_N$ values between 8 and 15. They both have moderate negative Eu anomalies (Eu/Eu* between 0.2 and 0.5), suggesting, together with the Sr and Ba negative anomalies (Fig. 6), plagioclase fractionation at the source. The LCS shows sub-horizontal, weakly fractionated patterns with $(La/Yb)_N$ values between 1 and 5, and very strong negative Eu anomalies (Eu/Eu* between 0.01 and 0.16).

According to major and trace element geotectonic discrimination diagrams, the compositions of the HG and SG are generally compatible with a post-orogenic setting. In the major element diagrams of Maniar and Piccoli (1989), both granites mostly plot in the post-orogenic granite field (Fig. 8). In the trace element diagrams of Pearce et al. (1984), the HG and the SG typically plot on or close to the triple junction of the volcanic arc, syn-collisional and within-plate granite fields (Fig. 9). This area of the diagrams is typical of post-orogenic or post-collisional granite compositions, as shown by the post-collisional granite field added by Pearce (1996) in the Rb versus Y + Nb diagram (Fig. 9), and discussed by Förster et al. (1997). In these trace element diagrams, the LCS plots in the within-plate granite field (Fig. 9). Figure 10 shows that the geochemistry of the studied granites is only partially similar to that of A-type granites (e.g. Whalen et al. 1987; Eby 1992). The studied granites have high Ga/Al ratios and Nb concentrations, comparable to those of A-type granites (Fig. 10). However, their Zn, Y, Zr and Ce concentrations (and the Zr + Nb + Ce + Y sum, used by Whalen et al. 1987, as a discriminator) are lower than the values considered typical of A-type granites and more similar to those of I- and S-type granites (Fig. 10).

The San Blas granite, in the north of the sierra, is characterized by a more mafic (SiO_2 = 68–71%), moderately peraluminous (A/CNK = 1.09–1.20) border facies and a felsic (SiO_2 = 74–76%), weakly peraluminous

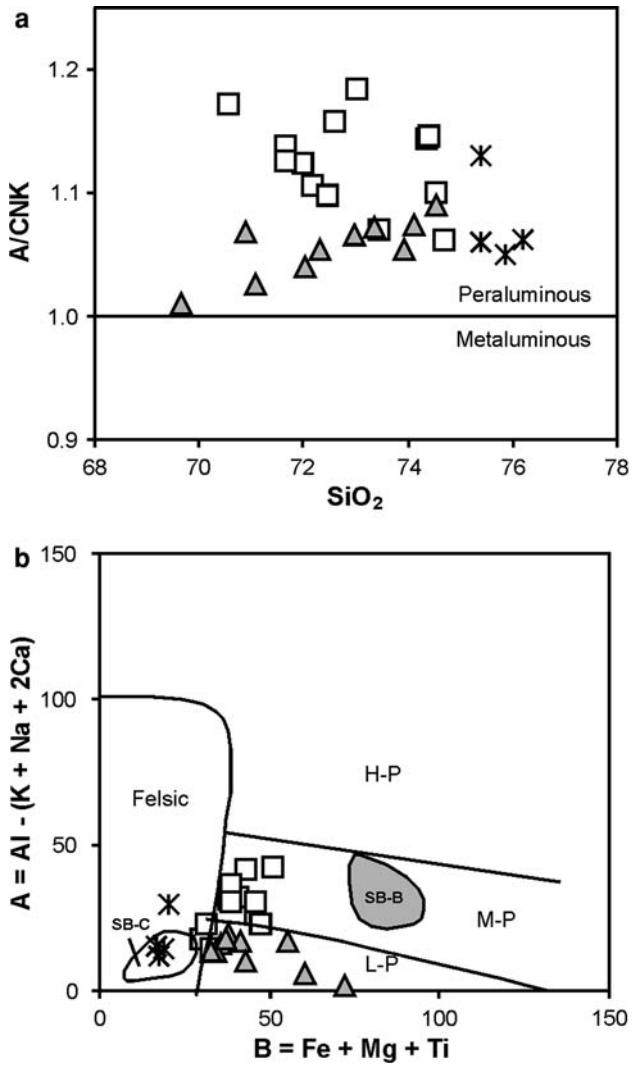

Fig. 4 **a** A/CNK versus SiO_2 diagram; **b** A–B diagram of Debon and Le Fort (1983) with the peraluminous granite classification of Villaseca et al. (1998a): H-P, highly peraluminous; M-P, moderately peraluminous; L-P, low peraluminous; Felsic, felsic peraluminous. *Symbols* as in Fig. 3. In **b** fields correspond to the two facies of the San Blas granite: SB-B, border facies; SB-C, central facies (data from 13 analyses of Báez (2006))

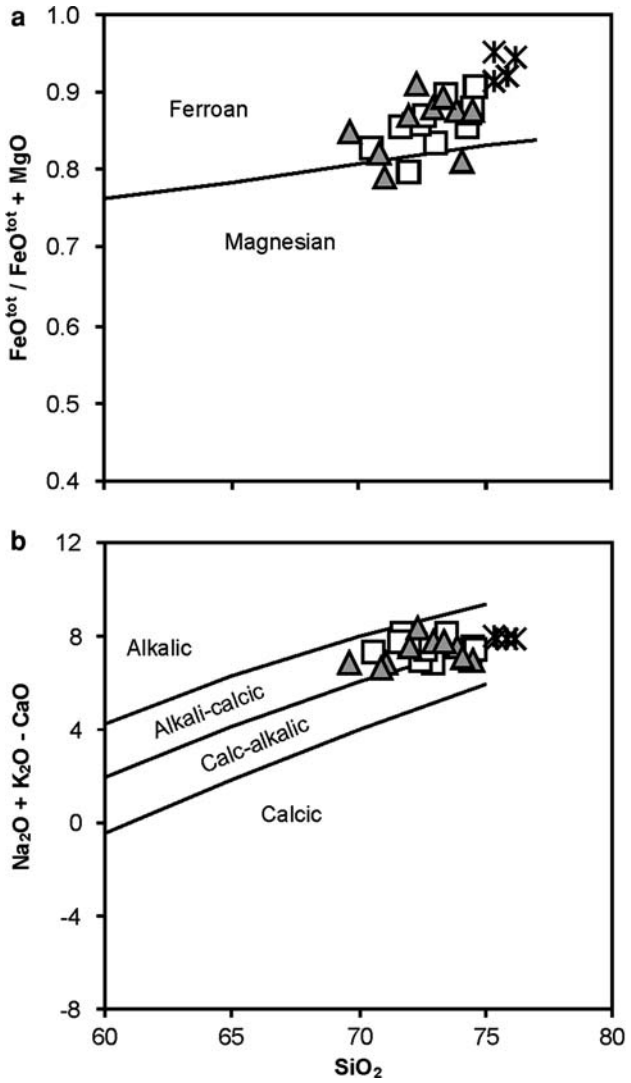

Fig. 5 Granite classification diagrams of Frost et al. (2001). **a** FeO^{tot}/(FeO^{tot} + MgO) versus SiO_2. **b** $Na_2O + K_2O - CaO$ versus SiO_2. *Symbols* as in Fig. 3

(A/CNK = 1.02–1.08) central facies (Báez 2006) (Table 2; Fig. 4b). This granite presents the same alkali-calcic, ferroan and K-rich affinity as the studied granites. The trace and REE element contents of the San Blas granite are more similar to those of the LCS than to those of the HG and SG (Table 2). As with the LCS, the San Blas granite has high concentrations in Rb, Th, U, Nb, Ta, Y and the HREE, and plots mostly in the within-plate granite field in the Pearce et al. (1984) diagrams. It can be distinguished from the LCS by its higher LREE contents and less pronounced negative Eu anomaly (Table 2).

The four analyzed mafic enclaves have very variable major element compositions that can be attributed to different degrees of hybridization with the host granite. Two enclaves have low SiO_2 contents of 55% and can be considered the least hybridized enclaves, while another has an intermediate SiO_2 content of 63% and the fourth has a high SiO_2 content of 70%. In comparison with the granites, the mafic enclaves have higher concentrations in ferromagnesian elements, CaO, Na_2O and P_2O_5, and lower K_2O contents. They are weakly to moderately peraluminous (A/CNK = 1.05–1.18). The mafic enclaves have trace element contents similar to the HG and the SG, although with higher concentrations in Zr, Y, the HREE and several transitional elements such as Sc, V and Zn (Table 2). They also produce similar REE patterns, but with somewhat lower $(La/Yb)_N$ values (5–10), due to higher HREE contents, and less pronounced negative Eu anomalies (Eu/Eu* = 0.25–0.34).

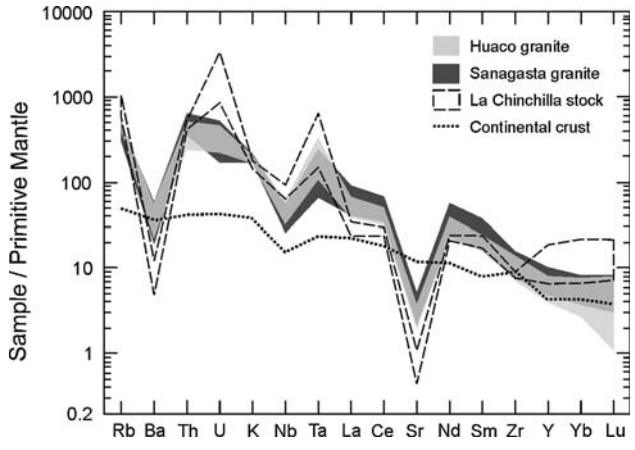

Fig. 6 Multi-element variation diagram, normalized to the primitive mantle (McDonough et al. 1992), of the studied granites (compositional fields) and of the continental crust (Taylor and McLennan 1985)

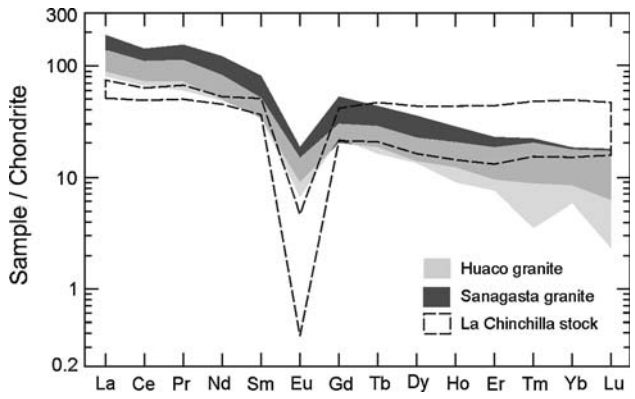

Fig. 7 Chondrite-normalized (Nakamura 1974) REE diagram of the studied granites (compositional fields)

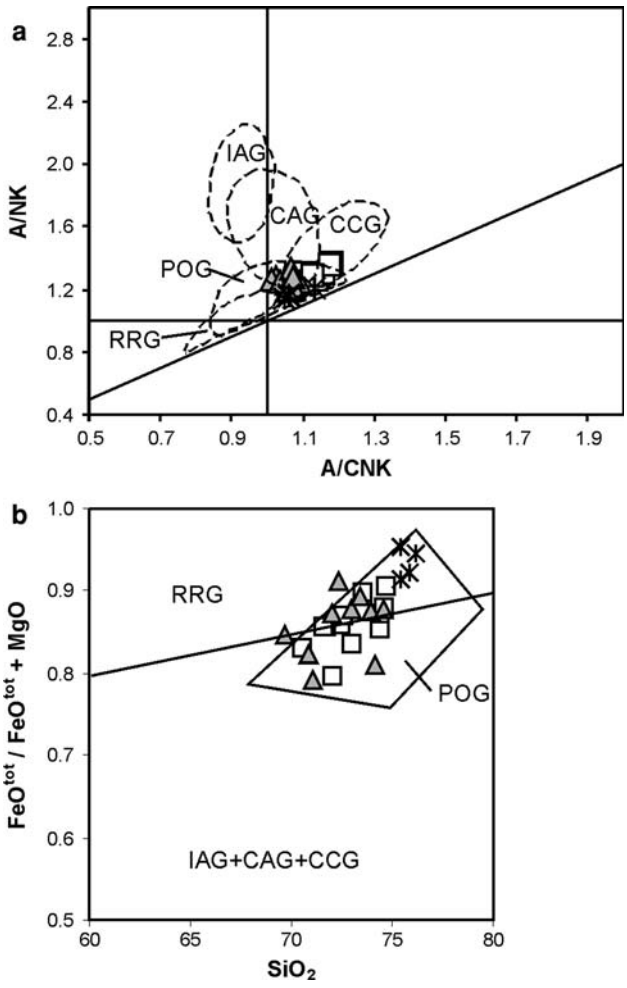

Fig. 8 Major element geotectonic discrimination diagrams of Maniar and Piccoli (1989). **a** A/NK versus A/CNK. **b** $FeO^{tot}/(FeO^{tot} + MgO)$ versus SiO_2. *Symbols* as in Fig. 3. Fields: *IAG* island arc granites, *CAG* continental arc granites, *CCG* continental collision granites, *POG* post-orogenic granites, *RRG* rift related granites

Nd isotopes

Table 3 shows 22 whole-rock Nd isotope analyses of the studied granites: eight analyses correspond to the HG, six to the SG, three to the LCS, two to mafic microgranular enclaves of the HG and SG, and three analyses are of the San Blas granite. The initial εNd values are calculated using the obtained U–Pb ages: 354 Ma for the HG, 353 Ma for the SG and 345 Ma for the LCS. For the mafic enclaves, the age of the host granite is considered, whereas for the San Blas granite the U–Pb SHRIMP age of 340 Ma obtained by Dahlquist et al. (2006) is used.

The HG and the SG have similar εNd values between −2.1 and −4.3 (average −3.3 ± 0.7). The LCS has somewhat higher εNd of −0.6 to −1.4, roughly comparable to the values shown by the San Blas granite (−1.4 to −1.7). The two analyzed mafic enclaves have even higher values of 0.6 and −0.6, suggesting a different, more primitive source.

Figure 11 is a diagram showing the initial εNd of the studied granites in comparison with values (recalculated to 350 Ma) of several potential crustal protoliths that outcrop in the Sierras Pampeanas (see figure caption for sources of data). It can be clearly seen that all of the potential crustal protoliths considered have lower εNd than the studied granites: the peraluminous S-type metagranitoids of Sierra de Velasco, and neighboring sierras of Copacabana and Fiambalá, have εNd between −5.5 and −7.4; the metaluminous I-type metagranitoids of southern Sierra de Velasco and Sierra de Chepes have εNd between −5.2 and −7.1; the low grade metasediments of the eastern flank of Sierra de Velasco and of other localities have εNd between −8.2 and −9.4; the medium to high grade metasediments of sierras of Aconquija and Quilmes have εNd between −4.7 and −9.6; and the medium to high grade metasediments of Sierra de Córdoba have εNd between −4.6 and −9.1. The more radiogenic εNd of the studied granites suggests that a more primitive component was involved in their genesis.

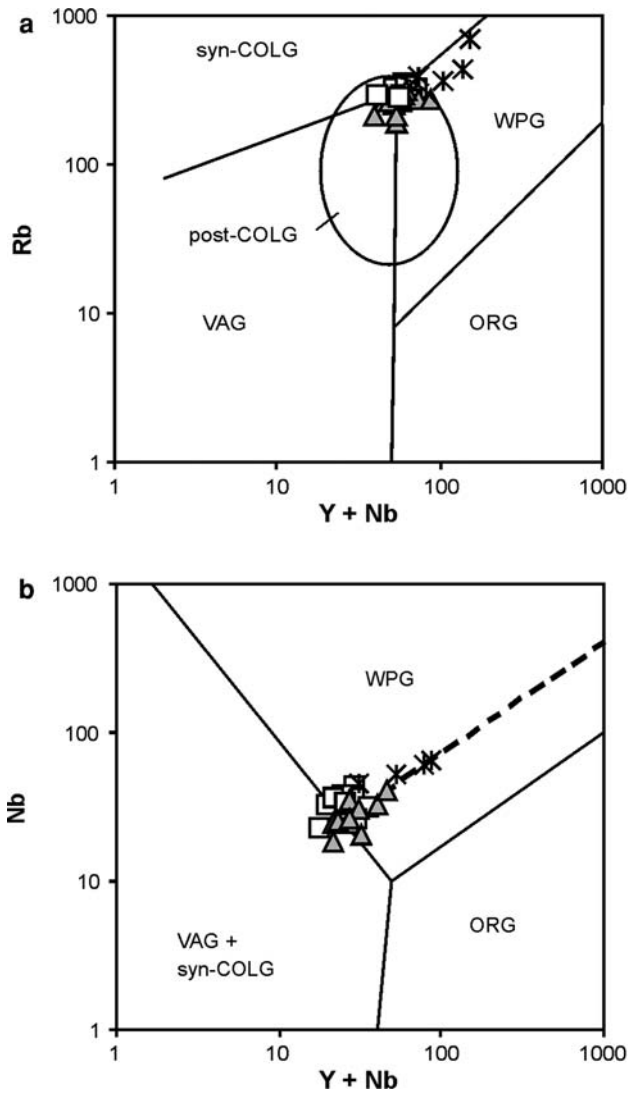

Fig. 9 Trace element geotectonic discrimination diagrams of Pearce et al. (1984).**a** Rb versus Y + Nb. **b** Nb versus Y. *Symbols* as in Fig. 3. Fields: ORG, ocean ridge granites; VAG, volcanic arc granites; Syn-COLG, syn-collisional granites; WPG, within-plate granite; the post-collisional field (post-COLG) in **a** is from Pearce (1996)

Nd model ages were obtained using one- and two-stage model calculations (Goldstein et al. 1984 and Liew and Hofmann 1988, respectively; see Table 3). The two-stage Nd model ages are considered more appropriate as it assumes an average Sm/Nd ratio for the crustal evolution prior to granite formation. Nd-model ages from crustal rocks can be seen as mixing ages representing different provenances of the source rocks. The two-stage model ages of the studied granites vary between 1,400 and 1,100 Ma (Table 3). These model ages are significantly lower than those determined for both I- and S-type Ordovician metagranitoids of neighboring ranges (~1,500–1,700 Ma; e.g. Pankhurst et al. 1998; Höckenreiner et al. 2003) and also lower than the typical values of the Proterozoic–Lower Paleozoic basement of the Sierras Pampeanas and of the southern Central Andes (~1,600–1,800 Ma, one-stage Nd model ages; e.g. Rapela et al. 1998; Bock et al. 2000; Lucassen et al. 2000). The higher εNd and lower Nd model ages of the studied granites compared to the Ordovician metagranitoids in particular, and the Proterozoic–Lower Paleozoic basement in general, can be explained by the participation of a Carboniferous depleted mantle-derived magma component in the generation of the granites. Taking into account that the non-detrital cores of zircons from the Huaco Granite are, without exception, Ordovician in age (Söllner et al. 2007), a Middle to Late Proterozoic crustal source for the studied granites can be discarded.

Sr isotopes

Sr isotopic ratios were determined for the same 22 samples analyzed for Nd (Table 3). The measured Sr ratios are very high and variable, defining pseudo-isochrons (not shown) with unrealistically old ages and low initial $^{87}Sr/^{86}Sr$ ratios. Even when recalculated for the time of crystallization using the U–Pb data, the initial $^{87}Sr/^{86}Sr$ ratios are high and variable (Table 3), suggesting incomplete Sr isotopic homogenization during melt generation and/or late- to post-magmatic disturbance of the Rb–Sr isotope system. Only the samples from the younger San Blas granite feature seemingly primary, homogeneous and low initial $^{87}Sr/^{86}Sr$ ratios (Table 3). Presentation of the data in a coupled Sr–Nd isotopic correlation diagram is inconsistent and confusing and hence, has been omitted.

The mafic enclaves have high initial $^{87}Sr/^{86}Sr$ ratios similar to their host granites (Table 3), suggesting an increase of their primary ratios due to interaction with the enclosing granitic melts. On the other hand, their εNd are considerably higher than those of the granites (Table 3; Fig. 11), suggesting that the enclaves were able to retain partly or totally their primary Nd isotopic ratios. This decoupling behavior between Nd and Sr isotopes is common in mafic enclaves (e.g. Holden et al. 1991; Lesher 1990, 1994; Pin et al. 1990; Allen 1991) and has been explained as a consequence of differences in diffusion velocities (e.g. Lesher 1994) or of retention of Nd in early crystallizing phases (e.g. Petford et al. 1996).

Discussion

Magma sources

The negative εNd values of the HG and the SG (between −2.1 and −4.3; see Table 3 and Fig. 11) suggests a mainly

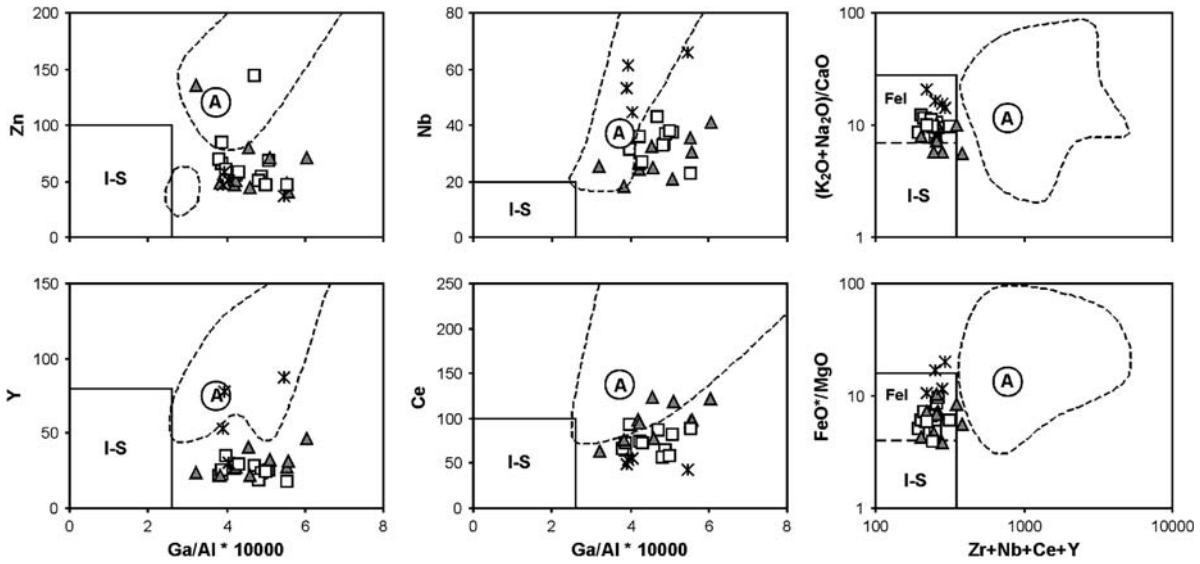

Fig. 10 Whalen et al. (1987) discrimination diagrams of A-type granites. Fields: I-S, I- and S-type granites; Fel, I- and S-type felsic and fractionated granites. *A* is the composition of the average A-type granite according to Whalen et al. (1987). *Dotted-line* fields are the compositional fields of 16 A-type granites studied by Eby (1992). *Symbols* as in Fig. 3

crustal source. In addition, the presence of non-detrital inherited cores with Ordovician ages in zircons of the HG (Söllner et al. 2007) strongly suggests that this crustal source consisted in Ordovician metagranitoids equivalent to those outcropping in the Sierra de Velasco. Other data compatible with a main crustal source for both granites are the high and restricted SiO_2 contents; the peraluminous character; the high concentrations in several typically crustal LIL elements such as Li, Rb and Cs; the low contents in CaO and ferromagnesian elements; and the lack of associated mafic intrusions.

However, the εNd values of the HG and the SG are clearly higher (and their Nd model ages are clearly lower) than the values of several potential crustal protoliths of the Sierras Pampeanas, and in particular of both the I- and S-type Ordovician metagranitoids (εNd values between −5.5 and −7.3; see Fig. 11). Thus, the participation of a more primitive component (i.e. a component with εNd values higher than those of the granites) is required to satisfy the Nd isotopic ratios. Although the origin of this more primitive material is unknown, it can be speculated that it consisted in mantle-derived melts, injected into the crust during crustal extension and mantle upwelling in a post-orogenic setting (see Sect. 7.2). Other data compatible with the participation of a more primitive component are the presence of mafic microgranular enclaves; the zircon typology corresponding to calc-alkaline granites of mixed crust-mantle origin (Pupin 1980); the calc-alkaline composition of biotites (Nachit et al. 1985); and the high concentrations in many HFS elements such as Nb, Ta and Th.

Comparison of the chemical compositions of the HG and the SG with experimental melts derived from crustal rocks is consistent with the participation of a more primitive and mafic component. In the A–B diagram of Debon and Le Fort (1983) (Fig. 12), the compositions of the studied granites are plotted together with the fields of experimental melts obtained from several lithologies, their respective starting materials, and the compositional fields of possible crustal protoliths outcropping in the region (see figure caption for sources of data).

The starting materials used in the felsic and mafic metapelite experiments are comparable, respectively, to the low-grade felsic metapelites and the higher-grade mafic metapelites that outcrop in the region (Fig. 12). The melts obtained from both types of metapelites are strongly peraluminous and leucocratic to mesocratic (Fig. 12). The strong peraluminosity of these melts and the generally lower CaO and ferromagnesian content is not compatible with the compositions of the HG and the SG. On the other hand, the metaluminous dacite used by Conrad et al. (1988), which is comparable to the I-type metagranitoids of the region, generates metaluminous to weakly peraluminous melts with varying ferromagnesian contents (Fig. 12). In the A–B diagram, these melts seem to have a somewhat similar composition to the SG (Fig. 12). However, the melts are much poorer in K_2O and richer in Na_2O and CaO than the SG, and, additionally, the εNd values of the I-type metagranitoids are clearly lower than those of the studied granites (see Fig. 11), implying that they can not be considered an exclusive source.

The metagreywackes used by Castro et al. (1999) and, in particular, the peraluminous orthogneiss used by Holtz and Johannes (1991) have similar compositions to the S-type Ordovician metagranitoids of the Sierra de Velasco

Table 3 Sm–Nd and Rb–Sr isotopic data of the studied granites and mafic enclaves of central-eastern Sierra de Velasco, and of the San Blas granite of northern Sierra de Velasco

Sample	Sm (ppm)	Nd (ppm)	$^{143}Nd/^{144}Nd$	Error 2 sigma	$^{147}Sm/^{144}Nd$	$\varepsilon Nd(T)$	Nd Model Ages		Rb (ppm)	Sr (ppm)	$^{87}Sr/^{86}Sr$	Error 2 sigma	$^{87}Rb/^{86}Sr$	$^{87}Sr/^{86}Sr$ (Initial, T)
							1[a]	2[b]						
Huaco granite (T = 354 Ma)														
6872	5.7	28.9	0.512274	0.000008	0.119	−3.60	1,363	1,346	330	62	0.81495	0.00005	15.5	0.737
6880	8.3	40.0	0.512305	0.000009	0.126	−3.31	1,414	1,323	329	58	0.82369	0.00004	16.7	0.740
6923	7.1	35.0	0.512345	0.000009	0.123	−2.40	1,307	1,252	–	–	–	–	–	–
6931	8.8	49.3	0.512237	0.000012	0.108	−3.83	1,280	1,364	290	81	0.78202	0.00002	10.4	0.730
7365	5.8	29.2	0.512355	0.000038	0.121	−2.10	1,259	1,228	269	46	0.83150	0.00005	17.3	0.744
7381	5.7	26.2	0.512284	0.000011	0.131	−3.94	1,530	1,372	329	54	0.83389	0.00004	17.8	0.744
7391	5.9	30.3	0.512268	0.000014	0.117	−3.63	1,345	1,348	294	42	0.85646	0.00003	19.8	0.752
7698	6.5	32.6	0.512243	0.000007	0.120	−4.27	1,430	1,398	280	55	0.81094	0.00001	14.8	0.737
Sanagasta granite (T = 353 Ma)														
7251	11.5	62.8	0.512296	0.000015	0.111	−2.80	1,225	1,282	275	72	0.78029	0.00002	11.1	0.724
7354	10.3	50.8	0.512350	0.000012	0.123	−2.29	1,294	1,242	318	79	0.79079	0.00002	11.8	0.732
7369	15.4	72.6	0.512312	0.000008	0.128	−3.27	1,437	1,319	276	97	0.76294	0.00003	8.31	0.721
7379	10.1	53.7	0.512296	0.000013	0.114	−2.95	1,263	1,294	296	88	0.77412	0.00006	9.79	0.725
7703	8.0	45.5	0.512221	0.000013	0.107	−4.08	1,281	1,382	213	89	0.75161	0.00001	6.96	0.717
7724	5.7	33.3	0.512220	0.000003	0.104	−3.98	1,251	1,374	215	77	0.76114	0.00002	8.06	0.721
La Chinchilla stock (T = 345 Ma)														
6916	8.7	24.5	0.512629	0.000016	0.214	−0.93	22,544	1,130	707	10	1.86289	0.00005	233	0.717
7738	7.1	24.3	0.512563	0.000010	0.176	−0.55	2,174	1,099	360	16	1.25905	0.00007	69.8	0.916
7740	9.2	30.8	0.512531	0.000008	0.181	−1.40	2,618	1,166	439	11	1.74322	0.00003	128	1.113
Mafic enclaves (T = 354 Ma)														
6885	11.9	64.8	0.512413	0.000010	0.111	−0.55	1,064	1,105	758	85	0.85864	0.00004	26.1	0.728
7734	9.5	73.2	0.512394	0.000012	0.078	0.61	830	1,016	356	49	0.86802	0.00005	21.5	0.760
San Blas granite (T = 340 Ma)														
6511	9.6	39.5	0.512452	0.000010	0.147	−1.46	1,513	1,167	496	34	0.90952	0.00005	43.0	0.701
6336	11.4	53.7	0.512398	0.000009	0.128	−1.72	1,292	1,187	594	66	0.83011	0.00003	26.4	0.703
6340	8.6	45.7	0.512364	0.000006	0.114	−1.74	1,160	1,189	460	56	0.82057	0.00003	24.0	0.704

εNd values calculated asuming $^{143}Nd/^{144}Nd\ (CHUR)_{today}$ = 0.512638 (Goldstein et al. 1984) and $^{147}Sm/^{144}Nd\ (CHUR)_{today}$ = 0.1967 (Peucat et al. 1988)

[a] Calculation of 1-stage model ages after Goldstein et al. (1984) with $^{143}Nd/^{144}Nd$ (DM) = 0.51315 and $^{147}Sm/^{144}Nd$ (DM) = 0.217

[b] Calculation of 2-stage model ages after Liew and Hofmann (1988) with $^{143}Nd/^{144}Nd$ (DM) = 0.513151, $^{147}Sm/^{144}Nd$ (DM) = 0.219 and $^{147}Sm/^{144}Nd$ (CC) = 0.12

(Fig. 12), which, as discussed above, can be considered the main crustal source of the HG and the SG. The experimental melts obtained from these lithologies are strongly to moderately peraluminous and leucocratic, their compositions differing from those of the HG and the SG (Fig. 12). The higher content in ferromagnesian elements and the lower peraluminosity of the HG and, in particular, the SG, compared to these experimental melts (Fig. 12), suggests additional participation of mafic material in the genesis of the granites. Castro et al. (1999) carried out melting-assimilation experiments between the metagreywackes and a gabbro as the mafic component. The resulting melts show a strong increase in ferromagnesian element contents and a decrease in peraluminosity that varies as a function of pressure. The hybrid melts produced at low-to-medium pressure are similar to the composition of the SG (Fig. 12). The composition of the HG could be obtained if (1) less quantity of the mafic component is assimilated; or (2) the assimilation process takes place at higher pressures. The later possibility is preferred to explain the compositional difference between the HG and the SG because both granites have similar εNd values and an equal abundance of mafic enclaves are observed in the field suggesting a similar proportion of crustal and mafic components. Different P–T conditions during fusion have been suggested, for example, by Villaseca et al. (1998b) to explain the compositional differences between two types of Hercynian peraluminous granites of Spain, referred to as PS- and

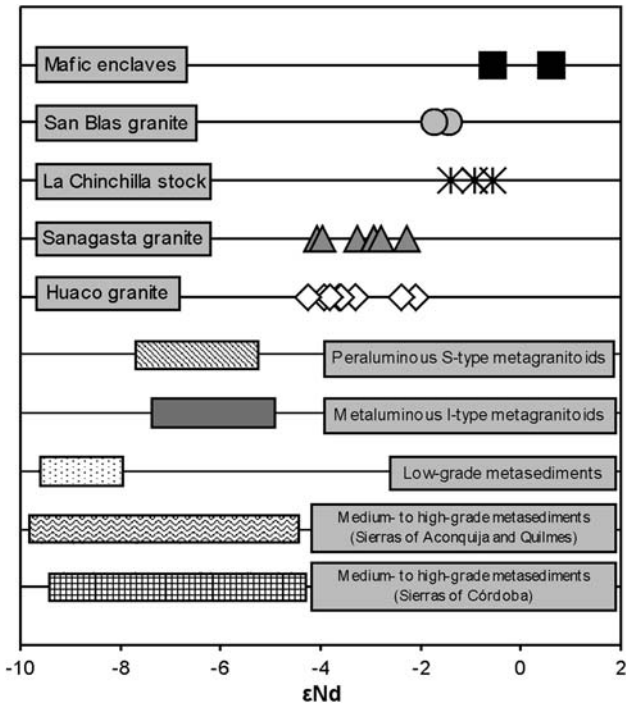

Fig. 11 εNd(T) values (T = intrusion age) of the Huaco, Sangasta, La Chinchilla and San Blas granites and of two mafic enclaves included in the Huaco and Sanagasta granites, and the ranges of εNd(T) values (T = 350 Ma) of potential crustal protoliths that outcrop in the Sierras Pampeanas: *peraluminous S-type metagranitoids* of sierras of Velasco, Copacabana and Fiambalá (9 samples from Höckenreiner et al. 2003; our unpublished data); *metaluminous I-type metagranitoids* of southern Sierra de Velasco and Sierra de Chepes (12 samples from Pankhurst et al. 1998; our unpublished data); *low-grade metasediments* of the eastern flank of Sierra de Velasco and from other localities (7 samples from Pankhurst et al. 1998; Bechio 2000; Höckenreiner et al. 2003; our unpublished data); *medium- to high-grade metasediments* of sierras of Aconquija and Quilmes (7 samples from Bechio 2000; our unpublished data); *medium- to high-grade metasediments* of Sierra de Córdoba (12 samples from Rapela et al. 1998). See text for further explanations

PI-types, that have similar εNd values. The composition of these granites are comparable to those of the HG and the SG, respectively.

The common mafic enclaves found in the HG and the SG, with εNd values close to zero (see Fig. 11), can be considered remnants of the more primitive mafic component. A possible mechanism for the assimilation of mafic enclaves by a granitic magma has recently been experimentally tested by García-Moreno et al. (2006). They have shown that dissolution of mafic enclaves in a granitic magma is a viable mechanism, specially during ascent of the magma, producing an increase in CaO, FeO and MgO in the granitic magma. They suggest that this mechanism is responsible for the generation of the "mixed series" monzogranites of the Central Extremadura Batholith of Spain. The similar composition of the HG and the SG with these granites, as well as the absence of contemporaneous input of mafic magmas and the lack of enclave-host granite Nd equilibration (García-Moreno et al. 2006), all seem to favor such a process.

The obtained data thus suggest that both the HG and the SG have a mixed source, composed by a main crustal source, consisting in Ordovician peraluminous metagranitoids, and a minor more mafic and primitive source, possibly mantle-derived. The main metagranitoid-derived melts assimilated the more mafic and primitive material, thereby reducing the peraluminosity and increasing the ferromagnesian element contents and εNd values of the resulting melts. Hybridization between crustal and mantle magmas has been proposed by López de Luchi et al. (2001, 2007) as a mechanism for the generation of Devonian granites in the Sierra de San Luis, which possibly belong to the same magmatic event as the studied granites (see Sect. 7.3).

The mineralogy (presence of albite, zinnwaldite and fluorite) and geochemistry (e.g. high SiO_2 and low CaO and ferromagnesian contents, high Rb/Sr and low K/Rb ratios, very strong negative Eu anomaly) of the LCS indicates that it is a highly evolved leucogranite and suggests fractionation by means of a F-rich fluid phase (e.g. Muecke and Clarke 1981; Dostal and Chatterjee 1995). Fluid fractionation with F as a complexing agent tends to produce strong enrichments in LIL and HFS elements (e.g. Taylor et al. 1981; Dostal and Chatterjee 1995; Irber 1999; Frindt et al. 2004), as is observed in the LCS (enriched in Li, Be, Y, Nb, Ta, U, the HREE). The LCS can be classified as a specialized granite, following the criteria of Tischendorf (1977), and is similar to the "P-poor" sub-type of topaz granites proposed by Taylor (1992) and to some A-type granites (e.g. Collins et al. 1982; Whalen et al. 1987).

The source of the LCS is difficult to determine due to its strongly evolved nature. This type of granite can be considered either as a final highly fractionated phase of a larger granite (e.g. Whalen and Currie 1990), i.e. the HG, or the product of melting of a different source (e.g. Manning and Hill 1990; Förster et al. 1995). The obtained data suggests that the LCS was generated from a different, more primitive source than the HG: its zircon typology is different from that of the HG and corresponds to that of alkaline granites of mantle origin (Pupin 1980); it has strong enrichments in many HFS elements such as Nb, Y, Pb and the HREE that do not follow the trends of the HG; and it has considerably higher εNd values (see Fig. 11).

The LCS and the San Blas granites share many characteristics (presence of fluorite, similar zircon typology, highly evolved nature, strong enrichments in many trace elements, high εNd values) which suggest that both of these granites originated from a similar source, more primitive or with a greater abundance of mantle-derived components

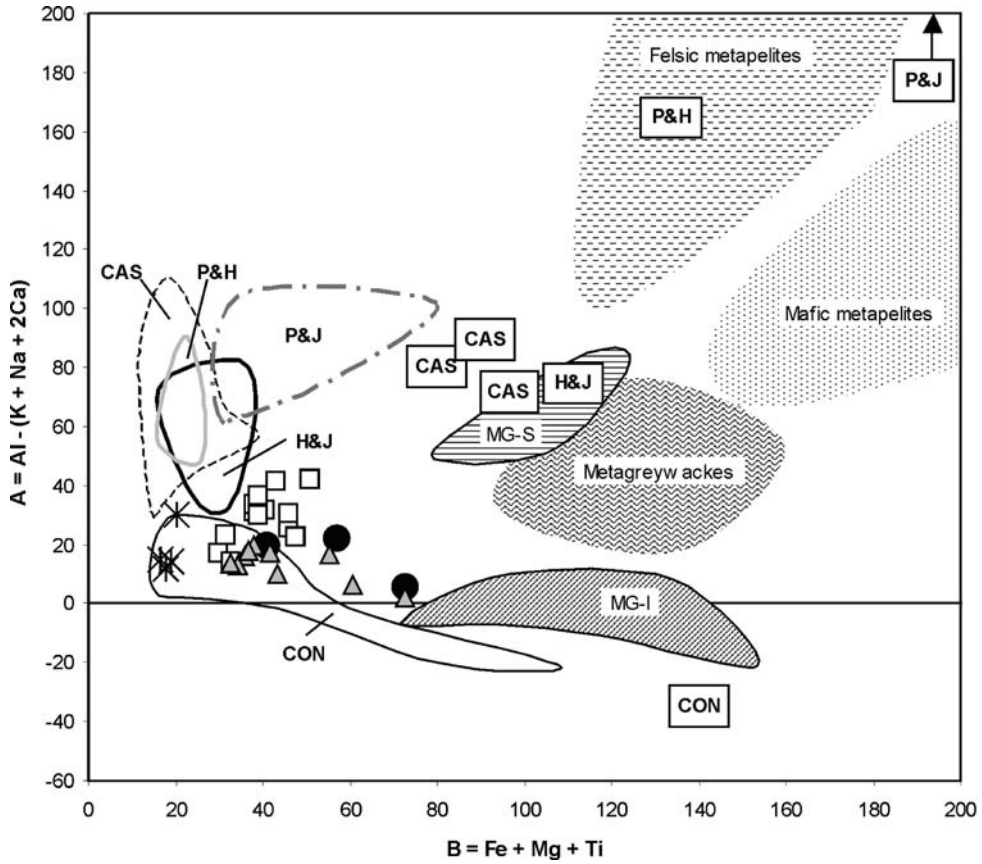

Fig. 12 A–B diagram with compositions of the studied granites (*symbols* as in Fig. 3) compared with experimental melts (*blank fields*), their respective starting materials (*rectangles*), and potential protoliths outcropping in the region (*solid fields*). The experimental melts and starting materials are: P&H, felsic metapelites of Patiño Douce and Harris (1998); P&J, mafic metapelites of Patiño Douce and Johnston (1991); CAS, peraluminous metagreywackes of Castro et al. (1999); H&J, peraluminous orthogneiss of Holtz and Johannes (1991); CON, metaluminous dacite of Conrad et al. (1988). The *black circles* are the melts obtained by 50:50 assimilation at low and medium pressures of metagreywackes with a gabbro (Castro et al. 1999). Potential protoliths are: *felsic metapelites* from sierras of Velasco and Ambato (Espizua and Caminos 1979; our unpublished data); more *mafic metapelites* from Sierra de Ancasti (Willner et al. 1990); *metagreywackes* from Sierra de Ancasti (Willner et al. 1990); S-type metagranitoids (*MG-S*) from Sierra de Velasco (Rossi et al. 2005; our unpublished data); I-type metagranitoids (*MG-I*) from Sierra de Velasco (Bellos 2005). See text for further explanations

compared to HG and the SG. The LCS and the San Blas granite are younger than the HG and SG by about 10–15 Ma, suggesting an increasing participation of primitive material with time during magma generation.

Geotectonic setting

Field relationships and the obtained Lower Carboniferous (~350 Ma) ages of the HG, SG and LCS clearly indicate that they are younger than the main Ordovician Famatinian magmatism (~460–490 Ma) and the deformation events that regionally affected the Ordovician metagranitoids and generated afterwards the spatially restricted mylonitic shear zones (e.g. Höckenreiner et al. 2003; Miller and Söllner 2005). If the age of 402 ± 2 Ma determined by Höckenreiner et al. (2003) is taken as the age of formation of the mylonites, and if these are interpreted as the result of a final compressive phase of the Famatinian orogeny (e.g. Miller and Söllner 2005), then the studied granites were generated approximately 50 Ma after this final compressive phase. This considerable age difference suggests that the studied granites are not orogenic (and thus are not related with active margin, collisional or post-collisional settings), but were instead generated during either a post-orogenic or anorogenic period, in both cases in a within-plate setting (following the classification scheme of geotectonic periods and settings of Liégeois 1998).

The geochemistry of the studied granites is more compatible with a post-orogenic period than with an anorogenic one. Their homogeneous compositions, high and restricted SiO_2 contents, high-K and alkali-calcic to calc-alkalic affinity, low to moderate peraluminosity and their generally moderate LILE and HFSE enrichments are characteristic of post-orogenic granites, such as the "Caledonian" granites of Pitcher (1983), the "post-orogenic" granites of Maniar

and Piccoli (1989) and the "high-K calc-alkaline" granites of Barbarin (1999). In particular, the studied granites are similar to the "post-orogenic alkaline granites (PA-type)" of Dawei et al. (1996) and to the "post-orogenic alkali-calcic granites with moderate LILE and HFSE enrichments" of Bonin et al. (1998).

The studied granites, specially the LCS and the San Blas granite, have several characteristics of A-type granites, such as a ferrous tendency (high Fe/Mg ratios), low CaO, MgO, Sr and Ba contents and high concentrations in certain trace elements such as Nb, Ta, HREE and Ga (e.g. Collins et al. 1982; Whalen et al. 1987; Eby 1990, 1992). However, the granites do not have alkaline tendencies, they are not metaluminous or peralkaline, and their HFS element concentrations are generally not high enough (in the sense of Whalen et al. 1987; see Fig. 10). Therefore, the studied granites are more comparable with post-orogenic A-type granites than with "true" anorogenic A-type granites. The partial similarity with A-type granites can be caused by the mixed origin of the studied granites, with some participation of mantle-derived material, which is considered predominant during the anorogenic period (e.g. Bonin 2004). The more primitive nature of the younger LCS and San Blas granite compared to the HG and the SG suggests an increasing mantle involvement with time and could be indicating a transition from a post-orogenic towards an anorogenic period.

The generation of the studied granites during a post-orogenic period implies a relationship with the previous orogeny. Thus, it can be considered that the studied granites were generated as a consequence of the extensional collapse of the Famatinian orogen. An extensional post-orogenic period, established during the collapse of the orogen (e.g. Dewey 1988), is favorable for the generation and emplacement of large granitic bodies (e.g. Barbarin 1999; Bonin 2004). Crustal extension during this phase favors mantle upwelling via slab-breakoff or slab-distortion (e.g. Davies and von Blanckenburg 1995), or delamination (e.g. Black and Liégeois 1993), which in turn favors crustal melting and magma generation due to its heat input. The crustal melts can also assimilate some of the mantle-derived material, as would have been the case of the studied granites. A further heat input could have been radiogenic heat from the previously thickened crust, as has been suggested for the generation of Variscan granites in Iberia (Bea et al. 1999) and Bohemia (Gerdes et al. 2000).

Regional implications

The obtained Lower Carboniferous ages of the HG, SG and LCS permits to correlate them with the Carboniferous San Blas and Asha granites of northern Sierra de Velasco (Fig. 1b). According to the existing U–Pb age data, these two granites have ages similar to the LCS, and they are approximately 10–15 Ma younger than the HG and the SG. Taken together, all of these granites occupy a total area of approximately 1,500 km^2 (25–30% of the Sierra de Velasco), demonstrating the importance of Lower Carboniferous magmatism in this region of the Sierras Pampeanas.

The obtained ages also allow to include the studied granites in the Middle Devonian to Lower Carboniferous granite group of the Sierras Pampeanas (i.e. the post-Famatinian or Achalian granite group). These granites are located along the previous Ordovician Famatinian magmatic arc and also to the east, both in central and eastern Sierras Pampeanas (Fig. 13). The HG and the SG share many characteristics with the granites of this group, such as nearly circular shapes, general lack of pervasive solid-state deformation, discordant relationships with the host rocks, shallow emplacement in the upper crust, syeno- to monzogranitic compositions, high SiO_2 and K_2O contents, porphyritic textures and abundance of pegmatites and aplites (e.g. Lira and Kirschbaum 1990; Grissom et al. 1998; Llambías et al. 1998; Pinotti et al. 2002; López de Luchi et al. 2007). These similarities suggest a common origin for the granites of this group. They were possibly generated during a regional crustal heating event (e.g. Miller and Söllner 2005) that occurred during a Late Devonian–Early Carboniferous post-orogenic period.

Granites with Devonian–Carboniferous ages confirmed by U–Pb geochronology are found in two main areas of the Sierras Pampeanas: southeast (sierras of Córdoba and San Luis) and north-central (sierras of Velasco and Fiambalá) (Fig. 13). In addition, other granites possibly belonging to this group crop out in the sierras of Vinquis and Zapata (e.g. Rapela et al. 1996), and in the sierras of Los Llanos, Chepes and Ulapes (according to unpublished field observations and mapping carried out by one of the authors, F. Söllner) (Fig. 13), although U–Pb age determinations of these granites are lacking.

The scarce existing U–Pb geochronological data suggests that the spatial distribution correlates with a temporal variation (Fig. 13). The southeastern granites have older, Middle to Upper Devonian ages, whereas the north-central granites have younger, Lower Carboniferous ages (Fig. 13). Even within the north-central area, there seems to be a general age decrease towards the north (Fig. 13). These U–Pb age variations suggest a possible northward migration of the magmatic activity, in a direction approximately parallel to the Ordovician Famatinian arc and to the main shear zones (Fig. 13). This possible migration could have been related to the mechanisms of magma generation. For example, it could be associated with a progressive delamination of the crust accompanied by upwelling of the upper mantle from south to north. The

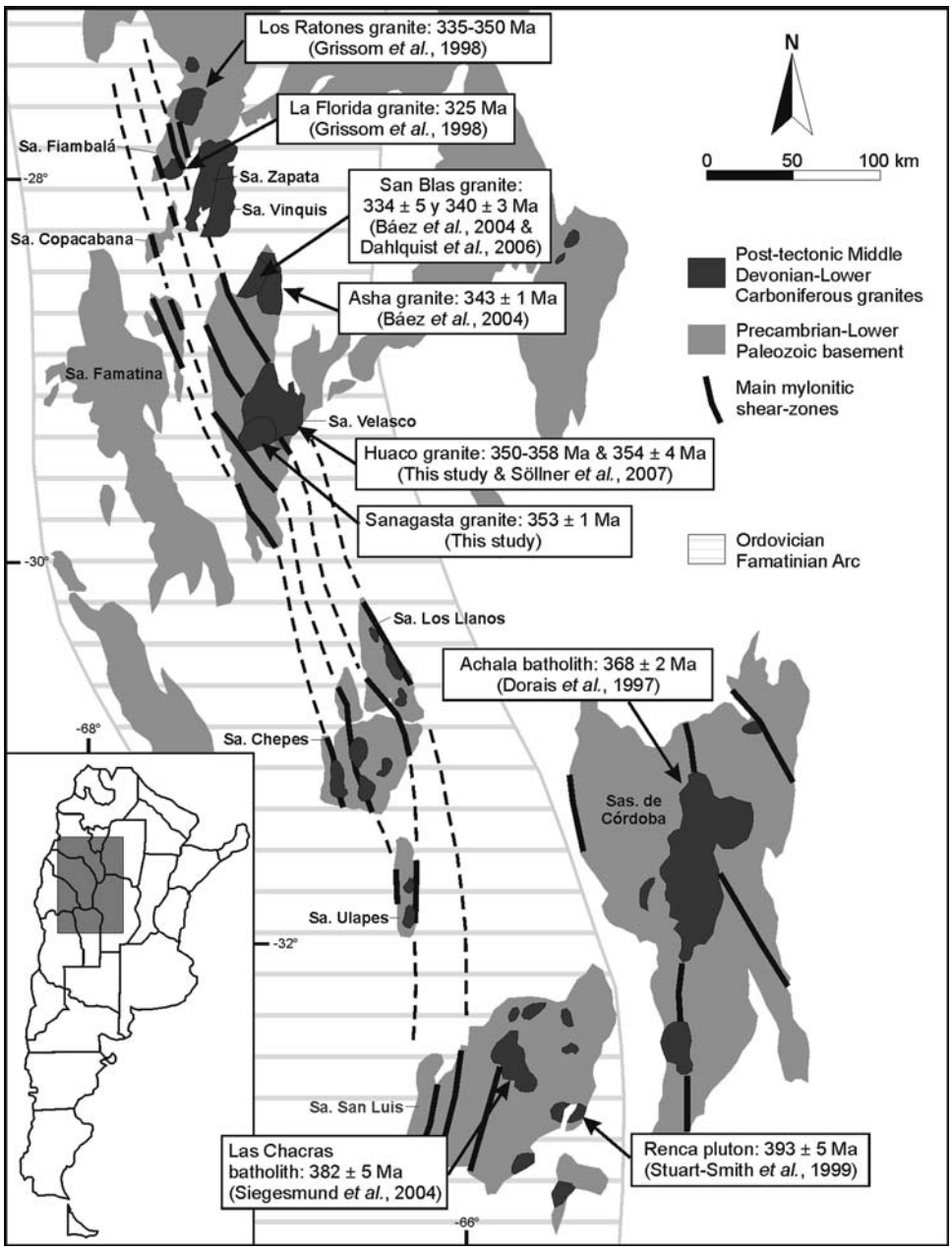

Fig. 13 Distribution of the Middle Devonian–Lower Carboniferous granites of the Sierras Pampeanas with existing U–Pb ages suggesting northward migration of the magmatism in a direction approximately parallel to the Ordovician Famatinian arc (modified from Pankhurst et al. 2000) and the main mylonitic shear zones

velocity of this magmatic migration can be calculated to about 10 km/Ma over a distance of more than 600 km and a time span of ~70 Ma. Further geochronological and geochemical data of this granite group is needed to verify this magmatic migration and identify its causes.

On the other hand, the studied Carboniferous granites cannot be deemed part of the Gondwanan Cycle (considered to extend from the Carboniferous to the Cretaceous; e.g. Pankhurst and Rapela 1998) because the Carboniferous Gondwanan granites (e.g. Llambías 1999), (1) are located far to the west, in the Cordillera Frontal, Precordillera and western Sierras Pampeanas; (2) are younger, mostly of Upper Carboniferous age; and (3) define a granodioritic to tonalitic calc-alkaline series typical of a subduction setting.

Conclusions

The data presented here allow to draw the following conclusions:

1. The central-eastern part of the Sierra de Velasco is composed by the undeformed Huaco and Sangasta

granites, and the La Chinchilla stock, of Lower Carboniferous age. These granites, together with the Carboniferous granites of the north of the sierra, make up about 25–30% of the sierra, indicating the importance of Carboniferous magmatism in this area, as opposed to previous studies which considered that the Sierra de Velasco consisted mostly in Famatinian inner-cordilleran S-type granites of Ordovician to Lower Devonian age (e.g. Rapela et al. 1992; Toselli et al. 1996; Pankhurst et al. 2000).

2. The HG and the SG have a mixed source, mainly crustal but with participation of a more primitive, possibly mantle-derived, component. The main crustal component can be attributed to Ordovician peraluminous metagranitoids such as those outcropping around the granites. The LCS, and the San Blas granite, derive from a more primitive source, suggesting an increase with time in the participation of the primitive component during magma genesis.
3. The studied Lower Carboniferous granites were generated during a post-orogenic geotectonic period in a within-plate setting. They were produced during a regional crustal heating phase in response to the collapse of the previous Famatinian orogen, extension of the crust and mantle upwelling.
4. The studied granites are part of the group of Middle Devonian–Lower Carboniferous granites of the Sierras Pampeanas. Many of these granites were probably generated during a post-orogenic period. The distribution and U–Pb ages of these granites suggest a northward arc-parallel migration of the post-orogenic magmatism with time.

Acknowledgments The Consejo Nacional de Investigaciones Científicas y Técnicas (CONICET) and the Deutscher Akademischer Austauschdienst (DAAD) are thanked for scholarships awarded to P. Grosse during his PhD studies. The Consejo de Investigaciones of the Universidad Nacional de Tucumán (CIUNT) is acknowledged for financial support through project 26/G321. Alex Rocholl is thanked for his help with Sm–Nd isotope separation. We thank Carlos Rapela and Siegfried Siegesmund for their thoughtful reviews which helped improve the quality of this article

References

Allen CM (1991) Local equilibrium of mafic enclaves and granitoids of the Turtle Pluton, southeast California: mineral, chemical and isotopic evidence. Am Mineral 76:574–588

Báez MA (2006) Geología, petrología y geoquímica del basamento ígneo-metamórfico del sector norte de la sierra de Velasco, provincia de La Rioja. Unpublished PhD Thesis, Universidad Nacional de Córdoba, p 207

Báez MA, Basei MA (2005) El plutón San Blas, magmatismo posdeformacional Carbonífero en la Sierra de Velasco. Serie Correlación Geológica 19:239–246

Báez MA, Rossi JN, Sardi FG (2002) Consideraciones preliminares sobre los granitoides del norte de la sierra de Velasco, La Rioja, Argentina. Proc XV Congreso Geológico Argentino 2:69–74

Báez MA, Basei MA, Toselli AJ, Rossi JN (2004) Geocronología de granitos de la sierra de Velasco (Argentina): reinterpretación de la secuencia magmática. Proc Simposio 40 años de geocronología en Brasil 1:85

Báez MA, Bellos LI, Grosse P, Sardi FG (2005) Caracterización petrológica de la sierra de Velasco. In: Dahlquist J, Rapela C, Baldo E (eds) Geología de la provincia de La Rioja -Precámbrico-Paleozoico Inferior. Asociación Geológica Argent Spec Publ 8:123–130

Barbarin B (1999) A review of the relationships between granitoids types, their origins and their geodynamic environments. Lithos 46:605–626

Bea F, Montero P, Molina JF (1999) Mafic precursors, peraluminous granitoids, and late lamprophyres in the Avila Batholith: a model for the generation of Variscan batholiths in Iberia. J Geol 107:399–419

Becchio R (2000) Petrología y geoquímica del basamento del borde oriental de la Puna Austral. Unpublished PhD Thesis, Universidad Nacional de Salta, p 128

Bellos LI (2005) Geología del sector sur de la sierra de Velasco, La Rioja. Serie Correlación Geológica 19:261–278

Bellos LI, Grosse P, Ruíz A, Rossi JN, Toselli AJ (2002) Petrografía y Geoquímica de Granitoides del flanco Sud-Occidental de la Sierra de Velasco, La Rioja, Argentina. Proc XV Congreso Geológico Argentino 2:81–86

Black R, Liégeois JP (1993) Cratons, mobile belts, alkaline rocks and continental lithospheric mantle: the Pan-African testimony. J Geol Soc Lond 150:89–98

Bock B, Bahlburg H, Wörner G, Zimmermann U (2000) Tracing crustal evolution in the Southern Central Andes from Late Precambrian to Permian with geochemical and Nd and Pb isotope data. J Geol 108:515–535

Bonin B (2004) Do coeval mafic and felsic magmas in post-collisional to within-plate regimes necessarily imply two contrasting, mantle and crustal, sources? A review. Lithos 78:1–24

Bonin B, Azzouni-Sekkal A, Bussy F, Ferrag S (1998) Alkali-calcic and alkaline post-orogenic (PO) granite magmatism: petrologic constraints and geodynamic settings. Lithos 45:45–70

Brogioni N (1987) El Batolito de Las Chacras-Piedras Coloradas, provincia de San Luis, geología y edad. Proc X Congreso Geológico Argentino 4:115–117

Brogioni N (1993) El Batolito de Las Chacras-Piedras Coloradas, provincia de San Luis, Geocronología Rb-Sr y ambiente tectónico. Proc XII Congreso Geológico Argentino 4:54–60

Castro A, Patiño Douce AE, Corretgé LG, de la Rosa JD, El-Biad M, El-Hmidi H (1999) Origin of peraluminous granites and granodiorites, Iberian Massif, Spain: an experimental test of granite petrogenesis. Contrib Mineral Petrol 135:255–276

Collins WJ, Beams SD, White AJR, Chappell BW (1982) Nature and origin of A-type granites with particular reference to southeastern Australia. Contrib Mineral Petrol 80:189–200

Conrad WK, Nicholls IA, Wall VJ (1988) Water-saturated and undersaturated melting of metaluminous and peraluminous crustal composition at 10 kb: evidence for the origin of silicic magmas in the Taupo Volcanic Zone, New Zealand, and other occurrences. J Petrol 29:765–803

Dahlquist JA, Pankhurst RJ, Rapela CW, Casquet C, Fanning CM, Alasino P, Báez MA (2006) The San Blas Pluton: An example of Carboniferous plutonism in the Sierras Pampeanas, Argentina. J South Am Earth Sci 20:341–350

Davies JH, von Blanckenburg F (1995) Slab breakoff: a model of lithosphere detachment and its test in the magmatism and

deformation of collisional orogens. Earth Planet Sci Lett 129: 85–102

Dawei H, Shiguang W, Baofu H, Manyuan J (1996) Post-orogenic alkaline granites from China and comparisons with anorogenic alkaline granites elsewhere. J Southeast Asian Earth Sci 13:13–27

de la Rosa JD, Chacón H, Sánchez de la Campa A, Carrasco R, Nieto JM (2001) Metodología y análisis de elementos trazas-REE mediante ICP-MS del standard SARM 1 granito y SARM 4 norita. Proc III Congreso Ibérico de Geoquímica 1:435–438

Debon F, Le Fort P (1983) A chemical–mineralogical classification of common plutonic rocks and associations. Trans R Soc Edinb Earth 73:135–149

Dewey JF (1988) Extensional collapse of orogens. Tectonics 7:1123–1139

Dorais MJ, Lira R, Chen Y, Tingey D (1997) Origin of biotite–apatite-rich enclaves, Achala batholith, Argentina. Contrib Mineral Petrol 130:31–46

Dostal J, Chatterjee AK (1995) Origin of topaz-bearing and related peraluminous granites of late Devonian Davis Lake pluton, Nova Scotia, Canada. Chem Geol 123:67–88

Eby GN (1990) The A-type granitoids: a review of their occurrence and chemical characteristics and speculations on their petrogenesis. Lithos 26:115–134

Eby GN (1992) Chemical subdivision of the A-type granitoids: petrogenetic and tectonic implications. Geology 20:641–644

Espizúa S, Caminos R (1979) Las rocas metamórficas de la Formación La Cébila, Sierra de Ambato, Provincias de Catamarca y La Rioja. Boletín de la Academia de Ciencias Córdoba 53:125–142

Förster H-J, Seltmann R, Tischendorf G (1995) High-fluorine, low-phospohrous A-type (post-collision) silicic magmatism in the Erzgebirge. Proc II Sympos Permocarboniferous Igneous rocks 7:32–35

Förster H-J, Tischendorf G, Trumbull RB (1997) An evaluation of the Rb vs. (Y + Nb) discrimination diagram to infer tectonic setting of silicic igneous rocks. Lithos 40:261–293

Frindt S, Haapala I, Pakkanen L (2004) Anorogenic Gross Spitzkoppe granite stock in central western Namibia: Part I. Petrology and geochemistry. Am Mineral 89:841–856

Frost BR, Barnes CG, Collins WJ, Arculus RJ, Ellis DJ, Frost CD (2001) A geochemical classification for granitic rocks. J Petrol 42:2033–2048

Galliski M (1993) La Provincia Pegmatítica Pampeana I: tipología y distribución de sus distritos económicos. Rev Geol Argent 49:99–112

García-Moreno O, Castro A, Corretgé LG, El-Hmidi H (2006) Dissolution of tonalitic enclaves in ascending hydrous granitic magmas: an experimental study. Lithos 89:245–258

Gerdes A, Wörner G, Henk A (2000) Post-collisional granite generation and HT-LP metamorphism by radiogenic heating: the Variscan South Bohemian Batholith. J Geol Soc Lond 157:577–587

Goldstein SL, O'Nions RK, Hamilton PJ (1984) A Sm–Nd study of atmospheric dusts and particulates from major river systems. Earth Planet Sci Lett 70:221–236

González Bonorino F (1951) Una nueva formación Precámbrica en el noroeste Argentino. Comunicaciones Científicas Museo de La Plata 5:4–6

Grissom GC, De Bari SM, Lawrence WS (1998) Geology of the Sierra de Fiambalá, northwestern Argentina: implications for Early Palaezoic Andean tectonics. In: Pankhurst RJ, Rapela CW (eds) The Proto-Andean margin of Gondwana. Geol Soc Lond Spec Publ 142:297–323

Grosse P, Sardi FG (2005) Geología de los granitos Huaco y Sanagasta, sector centro-oriental de la Sierra de Velasco, La Rioja. Serie Correlación Geológica 19:221–238

Grosse P, Larrovere M, de la Rosa JD, Castro A (2005) Petrología y origen del stock La Chinchilla, Sierra de Velasco, La Rioja (Argentina). Proc XVI Congreso Geológico Argentino 1:533–538

Grosse P, Rossi JN, Sardi FG, Toselli AJ (2006a) Química mineral de los granitos Sanagasta, Huaco y La Chinchilla, Sierra de Velasco, La Rioja, Argentina. Proc VIII Congreso de Mineralogía y Metalogenia 1:381–388

Grosse P, Rossi JN, Toselli AJ (2006b) Geoquímica de feldespatos y biotitas del granito orbicular de la Sierra de Velasco, La Rioja, Argentina. Proc VIII Congreso de Mineralogía y Metalogenia 1:373–380

Grosse P, Söllner F, Báez MA, Rossi JN, Toselli AJ, de la Rosa JD (2007) Petrology of post-tectonic granites in central-eastern Sierra de Velasco, NW Argentina. Proc XX Colloq Latin Am Earth Sci 1:31–32

Höckenreiner M, Söllner F, Miller H (2003) Dating the TIPA shear zone: an Early Devonian terrane boundary between Famatinian and Pampean systems (NW-Argentina). J South Am Earth Sci 16:45–66

Holden P, Halliday AN, Stephens WE, Henney PJ (1991) Chemical and isotopic evidence for major mass transfer between mafic enclaves and felsic magma. Chem Geol 92:135–152

Holtz F, Johannes W (1991) Genesis of peraluminous granites I. Experimental investigation of melt compositions at 3 and 5 kb and various H_2O activities. J Petrol 32:935–958

Irber W (1999) The lanthanide tetrad effect and its correlation with K/Rb, Eu/Eu*, Sr/Eu, Y/Ho, and Zr/Hf of evolving peraluminous granite suites. Geochim Cosmochim Acta 63:489–508

Lesher CE (1990) Decoupling of chemical and isotopic exchange during magma mixing. Nature 344:235–237

Lesher CE (1994) Kinetics of Sr and Nd exchange in silicate liquids: theory, experiments, and applications to uphill diffusion, isotopic equilibration, and irreversible mixing of magmas. J Geophys Res 99:9585–9604

Liégeois JP (1998) Preface—some words on the post-collisional magmatism. Lithos 45:xv–xvii

Liew TC, Hofmann AW (1988) Precambrian crustal components, plutonic associations, plate environment of the Hercynian Fold Belt of central Europe: indications from a Nd and Sr isotopic study. Contrib Mineral Petrol 98:129–138

Linares E, González RR (1990) Catálogo de edades radimétricas de la República Argentina 1957–1987. Asociación Geológica Argent Spec Publ 19, p 628

Lira R, Kirschbaum A (1990) Geochemical evolution of granites from the Achala batholith of the Sierras Pampeanas, Argentina. In: Kay S, Rapela CW (eds) Plutonism from Antartica to Alaska. Geol Soc Am Spec Publ 241:67–76

Llambías EJ (1999) Las rocas ígneas Gondwánicas: 1. El magmatismo Gondwánico durante el Paleozoico superior-Triásico. In: Caminos R (ed) Geología Argentina. Servicio Geológico Minero Argentino, Buenos Aires, pp 349–363

Llambías EJ, Sato AM, Ortiz Suárez A, Prozzi C (1998) The granitoids of the Sierra de San Luis. In: Pankhurst RJ, Rapela CW (eds) The Proto-Andean margin of Gondwana. Geol Soc Lond Spec Publ 142:325–341

López JP, Toselli AJ (1993) La faja milonítica Tipa: faldeo oriental del Sistema de Famatina, Argentina. Proc XII Congreso Geologico Argentino 3:39–42

López JP, Sales A, Basei MA (2000) Nueva edad K/Ar en la historia deformativa de la Faja Milonítica Tipa, en el Noroeste Argentino. Zbl Geol Paläont Teil I 7/8:895–902

López de Luchi MG, Siegesmund S, Hoffmann A, Hübner H, Hulka C, Mosch S (2001) Geological setting and composition of the Las Chacras-Potrerillos Batholith, Sierras Pampeanas, Argentina: first results. Z Dtsch Geol Ges 152:325–350

López de Luchi MG, Siegesmund S, Wemmer K, Steenken A, Naumann R (2007) Geochemical constraints on the petrogenesis of the Paleozoic granitoids of the Sierra de San Luis, Sierras Pampeanas, Argentina. J South Am Earth Sci 24:138–166

Lucassen F, Becchio R, Wilke HG, Franz G, Thirlwall MD, Viramonte J, Wemmer K (2000) Proterozoic–Paleozoic development of the basement of the Central Andes (18–26°S)—a mobile belt of the South American craton. J South Am Earth Sci 13:697–715

Ludwig KR (1994) PBDAT—a computer program for processing Pb–U–Th isotope data (version 1.24). US Geological Survey, Open-File Report, pp 88–542

Ludwig KR (2001) ISOPLOT/Ex version 2.49: a geochronological toolkit for Microsoft Excel. Berkeley Special Publication Centre, Spec Publ 1a

Maniar PD, Piccoli PM (1989) Tectonic discrimination of granitoids. Geol Soc Am Bull 101:635–643

Manning DAC, Hill PI (1990) The petrogenetic and metallogenetic significance of topaz granite from the southwest England orefield. In: Stein HJ, Hannah JL (eds) Ore-bearing granite systems; petrogenesis and mineralizing processes. Geol Soc Am Spec Publ 246:51–69

McDonough WF, Sun S, Ringwood AE, Jagoutz E, Hoffmann AW (1992) K, Rb and Cs in the earth and moon and the evolution of the earth's mantle. Geochim Cosmochim Acta 56:1001–1012

Miller H, Söllner F (2005) The Famatina complex (NW-Argentina): back-docking of an island arc or terrane accretion? Early Palaeozoic geodynamics at the western Gondwana margin. In: Vaughan APM, Leat PT, Pankhurst RJ (eds) Terrane processes at the margins of Gondwana, vol 246. Geol Soc Lond Spec Publ 246, pp 241–256

Muecke GK, Clarke DB (1981) Geochemical evolution of the South Mountain Batholith, Nova Scotia: rare-earth element evidence. Can Mineral 19:133–145

Nachit H, Razafimahefa N, Stussi JM, Carron JP (1985) Composition chimique des biotites et typologie magmatique des granitoides. CR Geosci 301:813–818

Nakamura N (1974) Determination of REE, Ba, Mg, Na and K in carbonaceous and ordinary chondrites. Geochim Cosmochim Acta 38:757–773

Northrup CJ, Simpson C, Hodges KV (1998) Pseudotachylite in fault zones of the Sierras de Córdoba, Argentina; petrogenesis and 40Ar/39Ar geochronology. Geol Soc Am Bull 30(7):325

Pankhurst RJ, Rapela CW (1998) The proto-Andean margin of Gondwana: an introduction. In: Pankhurst RJ, Rapela CW (eds) The Proto-Andean Margin of Gondwana. Geol Soc Lond Spec Publ 142:1–10

Pankhurst RJ, Rapela CW, Saavedra J, Baldo EG, Dahlquist JA, Pascua I, Fanning CM (1998) The Famatinian arc in the central Sierras Pampeanas: an early to mid-Ordovician continental arc on the Gondwana margin. In: Pankhurst RJ, Rapela CW (eds) The Proto-Andean Margin of Gondwana. Geol Soc Lond Spec Publ 142:343–367

Pankhurst RJ, Rapela CW, Fanning CM (2000) Age and origin of coeval TTG, I- and S-type granites in the Famatinian belt of NW Argentina. Trans R Soc Edinb Earth 91:151–168

Parrish RR (1990) U–Pb dating of monazite and its application to geological problems. Can J Earth Sci 27:1431–1450

Patiño Douce AE, Harris N (1998) Experimental constraints on Himalayan Anatexis. J Petrol 39:689–710

Patiño Douce AE, Johnston AD (1991) Phase equilibria and melt productivity in the pelitic system: implications for the origin of peraluminous granitoids and aluminous granulites. Contrib Mineral Petrol 107:202–218

Pearce JA (1996) Sources and settings of granitic rocks. Episodes 19:120–125

Pearce JA, Harris NB, Tindle AG (1984) Trace element discrimination diagrams for the tectonic interpretation of granitic rocks. J Petrol 25:956–983

Petford N, Paterson BA, McCaffrey KJW, Pugliese S (1996) Melt infiltration and advection in microdioritic enclaves. Eur J Mineral 8:405–412

Peucat JJ, Vidal P, Bernard-Griffiths J, Condie KC (1988) Sr, Nd and Pb isotopic systematics in the Archean low- to high-grade transition zone of southern India: syn-accretion vs. post-accretion granulites. J Geol 97:537–550

Pin C, Binon M, Belin JM, Barbarin B, Clemens JD (1990) Origin of microgranular enclaves in granitoids: equivocal Sr–Nd evidence from Hercynian rocks in the Massif Central (France). J Geophys Res 95:17821–17828

Pinotti LP, Coniglio JE, Esparza AM, D'Eramo FJ, Llambías EJ (2002) Nearly circular plutons emplaced by stoping at shallow crustal levels, Cerro Áspero batholith, Sierras Pampeanas de Córdoba, Argentina. J South Am Earth Sci 15:251–265

Pitcher WS (1983) Granite type and tectonic environment. In: Hsu K (ed) Mountain building processes. Academic Press, London, pp 19–40

Pupin JP (1980) Zircon and granite petrology. Contrib Mineral Petrol 73:207–220

Quartino B, Villar Fabre J (1962) El cuerpo granítico orbicular precámbrico de la Pampa de los Altos, sierra de Velasco. Rev Geol Argent 18:11–41

Rapela CW, Toselli AJ, Heaman L, Saavedra J (1990) Granite plutonism of the Sierras Pampeanas: an inner cordilleran Paleozoic arc in the southern Andes. In: Kay SM, Rapela CW (eds) Plutonism from Antarctica to Alaska. Geol Soc Am Spec Publ 241:77–90

Rapela CW, Pankhurst RJ, Kirschbaum A, Baldo EG (1991) Facies intrusivas de edad carbónica en el Batolito de Achala: evidencia de una anatexis regional en las Sierras Pampeanas? Proc VI Congreso Geológico Chileno 1:40–43

Rapela CW, Coira B, Toselli AJ, Saavedra J (1992) The Lower Paleozoic magmatism of southwestern Gondwana and the evolution of the Famatinian orogene. Int Geol Rev 34:1081–1142

Rapela CW, Saavedra J, Toselli AJ, Pellitero E (1996) Eventos magmáticos fuertemente peraluminosos en las Sierras Pampeanas. Proc XIII Congreso Geológico Argentino 5:337–354

Rapela CW, Pankhurst RJ, Casquet C, Baldo EG, Saavedra J, Galindo C, Fanning CM (1998) The Pampean Orogeny of the southern proto-Andes: evidence for Cambrian continental collision in the Sierras de Córdoba. In: Pankhurst RJ, Rapela CW (eds) The Proto-Andean Margin of Gondwana. Geol Soc Lond Spec Publ 142:181–217

Rapela CW, Casquet C, Baldo EG, Dahlquist JA, Pankhurst RJ, Galindo C, Saavedra J (2001a) Las Orogénesis del Paleozoico Inferior en el margen proto-andino de América del Sur, Sierras Pampeanas, Argentina. J Iberian Geol 27:23–41

Rapela CW, Pankhurst RJ, Baldo EG, Casquet C, Galindo C, Fanning CM, Saavedra J (2001b) Ordovician metamorphism in the Sierras Pampeanas: new U–Pb SHRIMP ages in central-east Valle Fertil and the Velasco Batholith. Proc III Simposio Sudamericano de Geología Isotópica 1:611–614

Rapela CW, Pankhurst RJ, Casquet C, Fanning CM, Baldo EG, González-Casado JM, Galindo C, Dahlquist J (2007) The Río de La Plata craton and the assembly of SW Gondwana. Earth Sci Rev 83:49–82

Rickwood PC (1989) Boundary lines within petrologic diagrams which use oxides of major and minor elements. Lithos 22:247–263

Rogers J, Adams J (1969) Geochemistry of uranium. In: Wedepohl K (ed) Handbook of geochemistry, sect II, vol 5. Springer, Berlin, pp 92E91–92E95

Romer RL, Rötzler J (2001) P–T–t evolution of ultrahigh-temperature granulites from the Saxon Granulite Massif, Germany. Part II: Geochronology. J Petrol 42:2115–2032

Rossi JN, Toselli AJ, López JP (2000) Deformación y metamorfismo en el noroeste de la sierra de Velasco, La Rioja, Argentina. Zbl Geol Paläont Teil I 7/8:839–850

Rossi JN, Toselli AJ, Báez MA (2005) Evolución termobárica del ortogneis peraluminoso del noroeste de la sierra de Velasco, La Rioja. Rev Geol Argent 60:278–289

Saavedra J, Baldo EG, Pankhurst RJ, Rapela CW, Murra J (1998) El granito Capilla del Monte (Sierras Pampeanas de Córdoba, Argentina): edad, geoquímica, génesis y especialización metalogénica. Proc X Congreso Latinoamericano de Geología 2:372

Salfity J, Gorustovich SA (1984) Paleogeografía de la cuenca del Grupo Paganzo, Paleozoico superior. Rev Geol Argent 38:437–453

Sardi FG (2005) Petrografía y caracterización de la mena del Distrito Pegmatítico Velasco, La Rioja, Argentina. Proc XVI Congreso Geológico Argentino 5:231–238

Sardi FG, Grosse P (2005) Consideraciones sobre la clasificación del Distrito Velasco de la Provincia Pegmatítica Pampeana, Argentina. Proc XVI Congreso Geológico Argentino 5:239–242

Schärer U (1984) The effect of initial 230Th disequilibrium on young U–Pb ages: the Makalu case, Himalaya. Earth Planet Sci Lett 67:191–204

Siegesmund S, Steenken A, López de Luchi MG, Wemmer K, Hoffmann A, Mosch S (2004) The Las Chacras-Potrerillos batholith (Pampean Ranges, Argentina): structural evidences, emplacement and timing of the intrusión. Int J Earth Sci 93:23–43

Sims JP, Ireland TR, Camacho A, Lyons P, Pieters PE, Skirrow RG, Stuart-Smith PG (1998) U–Pb, Th–Pb and Ar–Ar geochronology from the southern Sierras Pampeanas, Argentina: implications for the Palaeozoic tectonic evolution of the western Gondwana margin. In: Pankhurst RJ, Rapela CW (eds) The Proto-Andean Margin of Gondwana. Geol Soc Lond Spec Publ 142:259–281

Söllner F, Höckenreiner M, Miller H (2001) Constraints on the ages of Famatinian igneous intrusions and subsequent deformation in the Sierra de Fiambalá (Catamarca/NW-Argentina). Proc III Simposio Sudamericano de Geología Isotópica 1:624–627

Söllner F, Höckenreiner M, Miller H (2003) Age determinations and geochemical development of Early Devonian mylonite zones in NW-Argentina; La Rioja and Catamarca provinces. Proc XVIII Colloq Latin Am Earth Sci 1:72

Söllner F, Gerdes A, Grosse P, Toselli AJ (2007) U-Pb age determinations by LA-ICP-MS on zircons of the Huaco granite, Sierra de Velasco (NW-Argentina): a long-term history of melt activity within an igneous body. Proc XX Colloq Latin Am Earth Sci 1:57–58

Stacey JS, Kramers JD (1975) Approximation of terrestrial lead isotope evolution by a two stage model. Earth Planet Sci Lett 26:207–221

Steiger RH, Jäger E (1977) Subcomisión on geochronology: Convention on the use of decay constants in geo- and cosmochronology. Earth Planet Sci Lett 36:2359–2362

Stuart-Smith PG, Camacho A, Sims JP, Skirrow RG, Lyons P, Pieters P, Black L, Miro R (1999) Uranium–lead dating of felsic magmatic cycles in the southern Sierras Pampeanas, Argentina: implications for the tectonic development of the proto-Andean Gondwana margin. In: Ramos VA, Keppie JD (eds) Laurentia-Gondwana before Pangea. Geol Soc Am Spec Publ 336:87–114

Taylor RP (1992) Petrological and geochemical characteristics of the Pleasant Ridge zinnwaldite-topaz granite, southern New Brunswick, and comparisons with other topaz-bearing felsic rocks. Can Mineral 30:895–921

Taylor SR, McLennan SM (1985) The continental crust: its composition and evolution. Blackwell Scientific, Oxford, p 312

Taylor RP, Strong DF, Fryer BJ (1981) Volatile control of contrasting trace element distribution in peralkaline granitic and volcanic rocks. Contrib Mineral Petrol 77:267–271

Tischendorf G (1977) Geochemical and petrographic characteristics of silicic magmatic rocks associated with rare-element mineralization. In: Stemprock M, Burnet L (eds) Metallization associated with acid magmatism. Czechoslovak Geol Surv 2:41–96

Tischendorf G, Gottesmann B, Förster H-J, Trumbull RB (1997) On Li-bearing micas: estimating Li from electron microprobe analyses and an improved diagram for graphical representation. Mineral Mag 61:809–834

Toselli AJ, Durand FR, Rossi JN, Saavedra J, Sial AN (1996) Granitos peraluminosos de la Zona Batolítica Central de Sierras Pampeanas (NW Argentino): relaciones y significado geotectónico. Proc XII Congreso Geológico de Bolivia 2:755–768

Toselli AJ, Rossi JN, Sardi FG, López JP, Báez MA (2000) Caracterización petrográfica y geoquímica de granitoides de la Sierra de Velasco, La Rioja, Argentina. Proc XVII Colloq Latin Am Earth Sci, p 6 (CD)

Toselli AJ, Rossi JN, Miller H, Báez MA, Grosse P, López JP, Bellos LI (2005) Las rocas graníticas y metamórficas de la Sierra de Velasco. Serie Correlación Geológica 19:211–220

Toselli AJ, Rossi JN, Báez MA, Grosse P, Sardi FG (2006) El batolito Carbonífero Aimogasta, Sierra de Velasco, La Rioja, Argentina. Serie Correlación Geológica 21:137–154

Verdecchia SO, Baldo EG, Benedetto JL, Borghi PA (2007) The first shelly faunas from metamorphic rocks of the Sierras Pampeanas (La Cébila Formation, Sierra de Ambato, Argentina): age and paleogeographic implications. Ameghiniana 44:493–498

Villaseca C, Barbero L, Herreros V (1998a) A re-examination of the typology of peraluminous granite types in intracontinental orogenic belts. Trans R Soc Edinb Earth 89:113–119

Villaseca C, Barbero L, Rogers G (1998b) Crustal origin of Hercynian peraluminous granitic batholiths of Central Spain: petrological, geochemical and isotopic (Sr, Nd) constraints. Lithos 43:55–79

Whalen JB, Currie KL (1990) The Topsails igneous suite, western Newfoundland; fractionation and magma mixing in an "orogenic" A-type granite suite. In: Stein HJ, Hannah JL (eds) Ore-bearing granite systems; petrogenesis and mineralizing processes. Geol Soc Am Spec Publ 246:287–299

Whalen JB, Currie KL, Chappell BW (1987) A-type granites: geochemical characteristics, discrimination and petrogenesis. Contrib Mineral Petrol 95:407–419

Willner AP, Miller H, Jezek P (1990) Composición geoquímica del basamento sedimentario-metamórfico de los Andes del NW Argentino (Precámbrico superior-Cámbrico inferior). Serie Correlación Geológica 4:161–179